FINAL REPORT

NASA CONTRACT NAS8-40185

X-RAY TRANSMISSION MICROSCOPE DEVELOPMENT

Period of Performance
02/28/95-08/31/97

Principal Investigator
WILLIAM F. KAUKLER

Center for Microgravity and Materials Research
The University of Alabama in Huntsville
Huntsville, AL 35899

Table of Contents

1.0 Introduction

This Final Report covers the full contract period from February 28, 1995 to August 31, 1997 and summarizes the project and concludes the contract obligations.

With funding from the NASA MSAD Advanced Technology Development program, we have applied a state of the art microfocus (sub-micron) X-ray source, capable of 10 to 100 kV acceleration energies, to image by X-ray Transmission Microscopy (XTM), the solidification of metal alloys in real-time with resolutions of up to 5 μm. Magnified images were produced by projection radiography where the source spot size essentially determined the limit to resolution of the images. Since there were no 'optics', there was no focusing of the image required and thus one has infinite depth of field. Alloys were unidirectionally solidified in a horizontal furnace with X-ray transparent containment. The specimen and crucible were pulled at a controlled rate through a stationary temperature gradient. This arrangement maintained the solid-liquid interface within the field of the microscope for continuous viewing. The X-ray shadow (image) of the specimen was converted to a digital image for display and study. We have successfully imaged in real-time and (usually) for the first time: interfacial morphologies (such as cells and dendrites), nucleation, coalescence, incorporation of phases into the growing interface, and the solute boundary layer in the liquid at the solid-liquid (s/l) interface. We have also measured true local growth rates and can evaluate segregation structures in the solid. Many of these novel results will be provided in this report together with the technology advances of this project that enabled these discoveries to be made.

X-ray transmission (or shadow) microscopy relies on differential absorption of the X-ray beam to provide contrast. In the past, X-ray transmission microscopy has been employed for materials inspection but has lacked the resolution and contrast necessary for the study of microscopic solidification fundamentals. With state-of-the-art X-ray image converters and cameras, the 2-3% difference in X-ray absorption between crystalline and liquid aluminum produces sufficient contrast to observe the s/l interface. Only recently have high resolution X-ray sources, and high MTF* X-ray detectors advanced enough to allow the systematic study of the relationship between melt dynamics and the resulting microstructure. Imaging of metal solid-liquid interfaces in real-time with X-rays requires performance near the limit of technological feasibility. A picture of the Fein Focus High Definition X-ray System we used is shown at right (Figure. 1).

* MTF Modulation Transfer Function, a measure of the loss of resolution and contrast due to the passage of a signal (image) through a signal processing device. The function relates the outgoing signal (amplitude range) to the incoming as a function of the signal's frequency (e.g. line pairs per mm on the image). The smaller the features, the greater the signal loss - always. Imagine: an X-ray image starts with the 3% contrast of a s/l Al interface. After conversion to a digital image, the output contrast could be much less than 3%.

Interfacial features or morphologies which influence the functional properties of alloys generally form with dimensions less than 100 μm. These features have low differential absorption leading to very low contrast levels in their images. We are also forced to examine specimens thin enough (~1 mm) to identify discrete features since we are viewing the interface profile through the bulk. We can improve feature detectability by alloying the matrix material to enhance the local absorption at the microscopic level through high atomic weight solutes. Selection of appropriate solidification conditions and alloys enable the study of a multitude of solidification phenomena using the XTM.

A series of limitations reduce the number of methods available to perform microscopy on metals during solidification. One is the requirement for hard X-rays that can penetrate metals. Another is caused by the high temperatures needed to melt metal alloys. Yet another is the need to obtain high resolutions to begin to even see the features commonly found in solidifying alloys. If observations of exposed surfaces are made (e.g. with SEM or even polarized reflected light), the viewed microstructures will not be representative of those forming within the bulk.

The most frequent discussion of X-ray microscopy in the literature involves the diversity of ***soft*** X-ray microscopies, often using synchrotron sources or lately, pulsed laser plasmas. With these, the desire is more to break the visible light resolution barrier of conventional optics by employing the shorter wavelength of X-rays. Most of these methods employ scanning techniques which can only be used with stationary subjects. However, the hard X-rays needed to see inside metals *cannot* be refracted to a focus by a lens. Hence, as discussed in section 1.1, one utilizes the projection of the object with X-rays originating from a micro-focus source.

The XTM is also a valuable tool for post-solidification metallography. Without the cumbersome furnace housing and crucible, specimen examination is possible with higher magnification (over 800 X), higher resolution and contrast since the specimen can be placed close to the source, and longer exposures used to achieve higher signal to noise ratios. Distribution of solute and solidification features within the specimen volume can be viewed without sectioning or other treatment when the solute has sufficiently higher atomic mass than the solvent. With an XTM available on the Space Station or Shuttle as part of an X-ray furnace facility, one could employ the XTM for metallography (or any material examination) without having to section, grind and polish the specimen first. An optical microscope would be a worthwhile addition to an orbital research facility, but the headaches of using and disposing etching acids, wash water and unbound abrasives in microgravity presently preclude their use and consequently quash the numerous experiments one could perform in space.

1.1 How it Works

Micro-focused X-ray tubes for projection radiography use high-voltage-accelerated electrons in a high vacuum focused a small spot typically onto a tungsten target. Refer to Fig. 2. To be considered micro-focused, the spot diameter is < 100 micrometers. Brehmstrahlung X-rays radiate from that spot in all directions. Their energy is non-monochromatic i.e. it covers a spectrum. By intercepting the radiated 'beam' with a specimen, it is differentially absorbed depending on local density, and passes through to cast an X-ray shadow. The shadow image is converted to visible light. With a phosphor or scintillator material, this converted X-ray image can be transformed to an electronic image by coupling the scintillation screen to a camera and recording the events on video tape or as digital images in a computer. One might also use film to convert the image if real-time information or specimen motion are not issues.

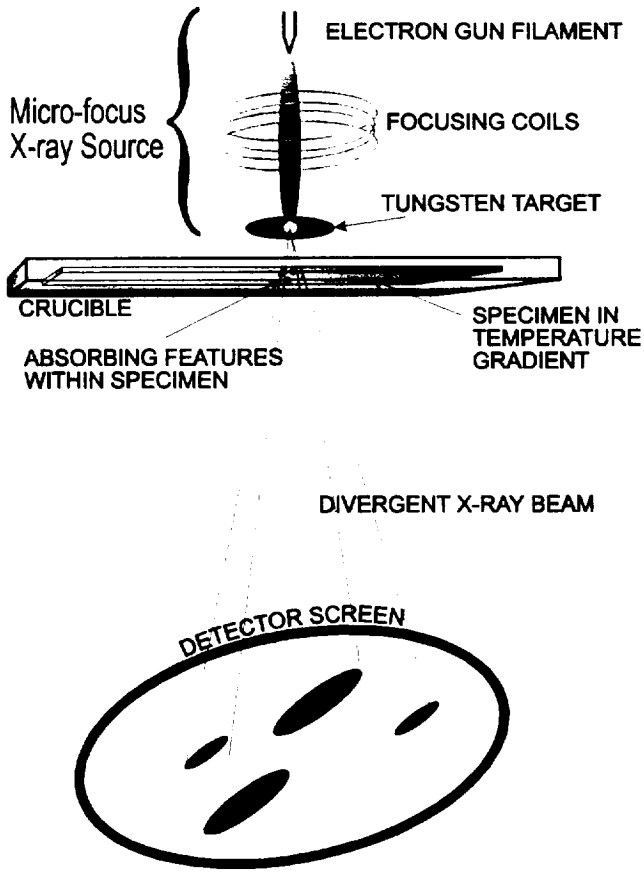

Figure 2. X-ray Transmission Microscope for solidification studies schematic diagram showing image projection from micro-focus source.

Placing the screen farther away expands the image since the 'beam' diverges. This produces magnification that that can be used for X-ray microscopy. The spot size practically determines the resolution, see Figure 3. This figure also demonstrates how magnification is calculated.

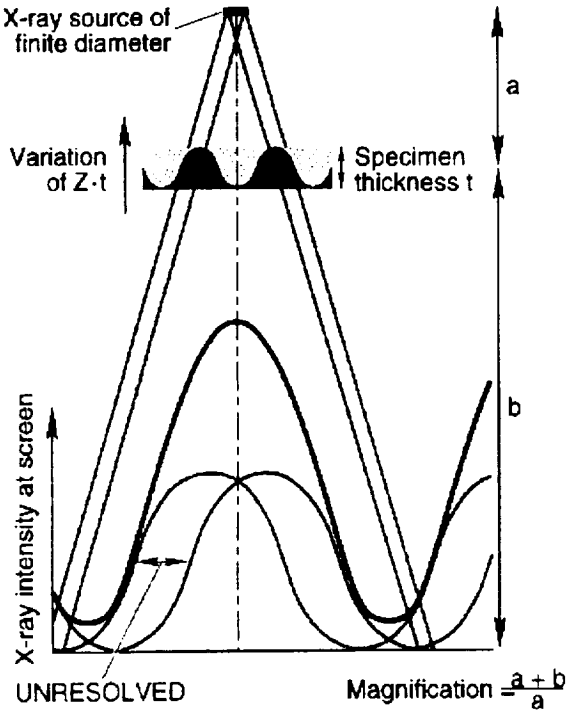

Figure 3. Limitation to resolution by spot size.

To obtain the best images, contrast must be preserved through the imaging train. High resolution is not itself a guarantee of good

results. Degradation of the image contrast occurs because of the image conversion and display processes that occur after the X-ray shadow image is produced. Figure 4 illustrates the problem of contrast loss due to noise. One must realize that any imaging system tends to lose information with high spatial frequency. The MTF is used to describe the loss. This diagram shows how small features tend to be lost as a result of processing the X-ray image to make it visible. Since the scintillator screen needed to convert the X-rays diffuses the image, it reduces the MTF or the contrast of the smallest image details. The technologies selected can optimize the system to obtain the best images for the conditions desired. For example, film offers an excellent MTF and contrast, but at the expense of long exposures due to a low sensitivity. An intensifier adds noise to the image and cuts off the high frequency data, but offers real-time viewing. The dynamics of solidification require real-time capable detectors and so we live with the loss of resolution and contrast. Fortunately, by magnifying the image the high frequency data is lowered in frequency and is more easily detected. Taken as a whole, all the characteristics produce, when optimized, the kind of images shown in the following and skirt the envelope at the limits of the technology.

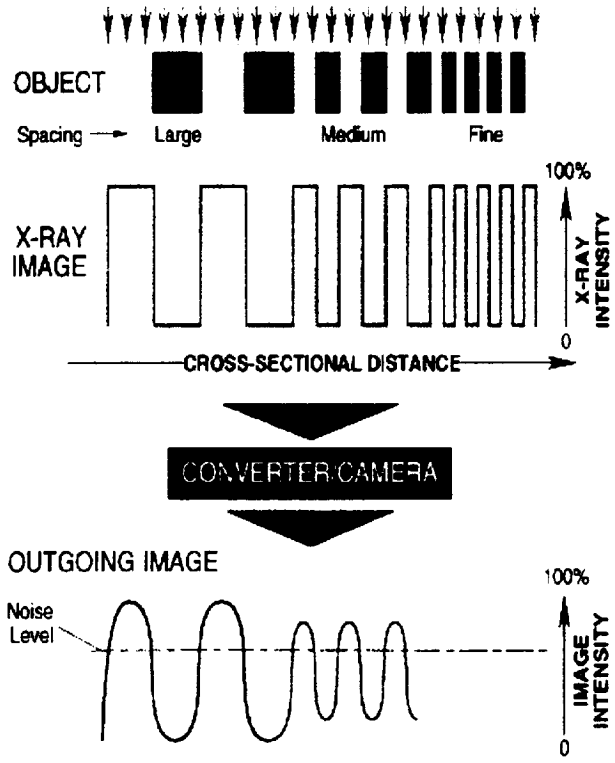

Figure 4. Limitation of contrast due to feature size.

2.0 Project Objectives

The objectives of the NASA ATD that funded this effort comprise the development of an X-ray Transmission Microscope (XTM) for the in-situ and real-time observation of interfacial processes in metallic systems during solidification.
Below are the performance goals established before the project was begun. All of them have been met or exceeded.

The XTM for solidification studies should have the following capabilities:

1. provide a resolution for specimen features of 10-100 μm,
2. at solidification rates of 0.1 to 20 μm/sec,
3. temperatures up to 1100 C with temperature gradients up to 50 C/cm,
4. with contrast sensitivities sufficient to detect 2-5% difference in absorptance,
5. offer 1, 2 and 4 in exposure times of a few seconds, and
6. permit recording of stereo pairs for depth information.

2.1 Project Significance to the MSAD Science Program

Physical processes which occur at, or near, interphase boundaries during solidification or other phase transformations, play a major role in the determination of many of the technologically important properties of solids. To-date, interfacial morphologies and particle-interface interactions in the respective metallic, optically opaque systems have been deduced from post-process metallographic analyses of specimens. Thus, little information is obtained about the detailed dynamics of the processes. These investigations have been considerably augmented by real-time observations of transparent materials; yet, since some of the interfacial and transport properties of these materials differ greatly from those of metals and semiconductors the results are not necessarily representative of these opaque systems.

The purpose of this project was the development of a high resolution X-ray microscope to view, in-situ and in real time, interfacial processes in metallic systems either during freezing or solid-solid transformations.

Precise control over solidification processes is acquired through improvement of the theory applied. Experimentation to refine the mathematical models require precise knowledge of all pertinent parameters that define the model and to do so during the dynamic processes of heat and mass transport during solidification.

Low-gravity damping of convective transport as a means to simplify experimental conditions has been pursued with some enthusiasm by the solidification science community. However, the cost of microgravity experiments is very high. Progress in some of the most critical areas of solidification and crystal growth systems utilizing microgravity, has been limited due to a lack of precise knowledge of the fundamental solidification variables. This necessitates, now more than ever, that space experiments be designed with the highest scientific yield.

Unambiguous testing of current alloy solidification models requires precise knowledge of the shape and extent of the solute boundary layer, real local growth rate, solid-liquid interfacial

morphology, as well as formation of the different phases. Experiments that rely on post solidification microstructural and compositional analysis provide only an indirect assessment of these critical variables. A common interfacial marking technique, Peltier Pulsing, disturbs the solidification processes. Interface quenching gives data only at the time of interruption of the solidification process.

A microfocus X-ray capability in orbit would provide better fundamental data for a number of current discipline areas in microgravity materials science. Some examples are particle pushing in composites, semiconductor crystal growth and diffusion experiments.

3.0 X-Ray Source Evaluation

In a word, the performance of the High Definition (Fein Focus Inc.) X-ray source was superb. After installation and some fine tuning, the device was shown to be an excellent performer that in some ways exceeded advertised specifications.

3.1 X-ray Source Characterization

Using the supplied tri-focus X-ray image intensifier, and the borrowed gold line resolution grid, it was ultimately possible to resolve the 2 micron lines on the grid in real time. It became clear that to achieve the highest resolutions possible from this instrument, limited by the intensifier, one needed to maintain the specimen placement within the first 4 to 5 mm nearest the source. The magnifications exceeded 500 X when specimens were placed with the nearest mm to the target. The grid was radiographed on Dupont 55 film and showed clearly the 2 micrometer lines. The clarity was so good that it can be assumed the resolution approaches 1 micrometer or better (with film). What was unexpected was that this resolution was available at the maximum power the machine would operate with. In the last year of the project, an Al-Bi monotectic alloy was solidified to produce droplets or particles in regular arrays. Some of these particles were smaller than 3 μm in diameter. Images of these particle arrays on X-ray film clearly resolve the particles *and* where the particles appear to overlap in the image, they are so clearly resolved one can see true 1 μm resolution.

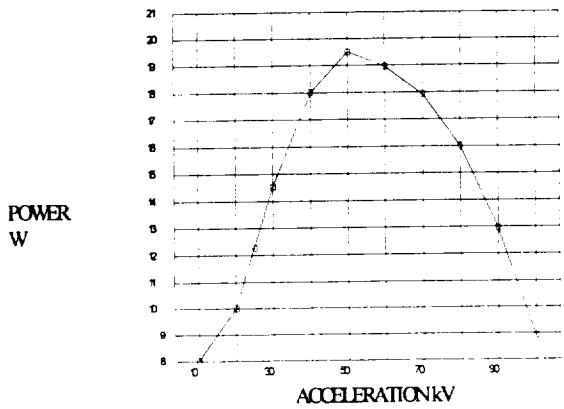

Figure 4. Fein Focus Inc. High Definition tube maximum power vs. electron acceleration over the full acceleration range.

The input acceleration of 50 kV and 400 microamps offered 20 watts of input power. Due to internal computer imposed limitations, the power level drops off on either side of this point. The maximum power input was determined and is plotted in Figure 4. At this time, the reason for power drop off below 50 kV is not known. Above 50 kV, the 5 micrometer thick W target is protected by cutting the current as acceleration increases.

From prior communications with Fein Focus Inc. the power density of electrons onto the target was ostensibly determined by the limitations of damaging the W target given a limit to the removal of excess heat. The curves for the other machines they build approximately showed a linear relation with power level in watts and the same figure for the minimum focal spot size in micrometers (i.e. a 10 micron spot could tolerate 10 watts of power, and a 1 micron spot only 1 watt of power maximum). For the performance levels of resolution desired (sub-micron spot size), a low X-ray power would be expected. It seems that the electron optics of this High Definition tube significantly reduce the electron flux to the focus spot during the beam

conditioning process. As a consequence, it has been observed that after prolonged operation (1 hour) at maximum power, the outer target surface was merely warm to the touch. Compare this to the uncomfortably high heat emanating from the other transmission tube target used for the feasibility studies not even operating at full power. This evidence supports the deduction that the power of the electron beam reaching the target is far less than that being generated at the filament. On the other hand, external cooling, not offered by the manufacturer had to be added to the tube due to the gradual build-up of heat from the focusing coils. Experiments running over an hour with the tube on full time, would cause the tube body to overheat (above 110 F) and it would cut out for quite some time (if not actively cooled). Now, the cooling loop for the furnace includes the X-ray source just prior to draining to the circulator.

A variety of specimen types were examined with interesting results. For example, real-time observation through 1 mm of tin or HgCdTe was not possible. Thin chips of BiSrCuO high T_c superconducting material were equally difficult to image. Thin sheet metal boxes made from steel, copper, brass or nickel did not prevent detection of the contents. Nickel beads of 30-100 micrometer diameter were easily imaged in real time and could be detected through 6 mm of Al. This showed the high contrast was available when such beads will be used for particle pushing experiments. Five mm diameter specimens grown in the ADSF furnace were examined. Iron and steel specimens did not reveal any interesting structures. However, old specimens of Al-In-Sn alloys were proving very interesting and the X-ray microscope views provided far more information than any metallography could ever have permitted. So, the limited power of the source is not a significant problem.

The higher resolution and contrast offered by film radiography was explored with exemplary results. The near infinite depth of field the X-ray source offers permits views of materials few people have seen. The one micrometer (at the film) resolution of the radiographic film does not limit the image quality of any specimen in this instrument. Images as clear as those obtained from contact radiographic methods were obtained.

Measured Characteristics of Fein Focus Inc. High Definition Tube

Part of the characterization of the instrument carried out was the measurement of certain important variables that were not supplied by the Fein Focus Inc. people. Examples are output fluxes, magnification range, resolutions, power level and more as a function of acceleration voltage, current, and specimen to detector geometry.

A set of measurements were made to determine the magnification available.

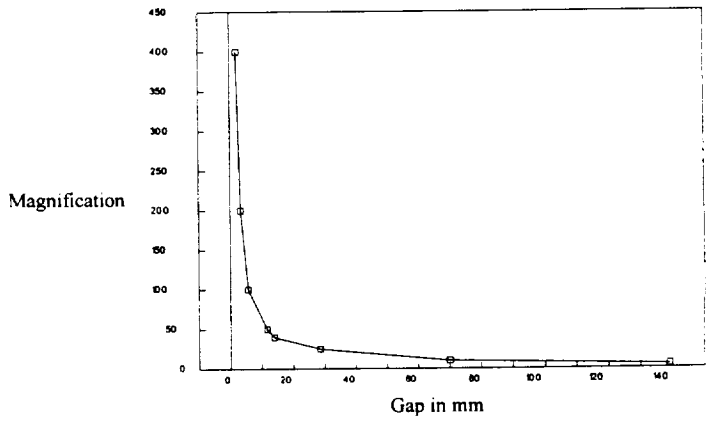

Figure 5. Magnification vs. distance from target surface at image intensifier.

The measurements were compiled in a graph where the source and intensifier positions are fixed (as they usually are). The calibrated wires and bars used to make the measurements were extremely precise and errors of a thousandth of an inch are the most one will see. The magnification as a function of distance from the target or window's exterior onto the intensifier is plotted in Fig. 5. As one can see, the significant magnification can only be achieved within the first 5 mm (1/4 of an inch) from the target. True for the fixed distance from target to intensifier tube of 21 inches. The measurements could not be made higher than the graph shows although 800 X was achieved by another means. An important consequence is the high significance of the relative depth of the features within the specimen when the specimen is in this 5 mm zone. A 1 mm specimen, such as the kind anticipated for solidification studies can have a features displayed several hundred times different in magnification. This will not be as great a problem in the furnace since the furnace walls will impose a gap of at least 3 mm, some magnification difference will occur but not as unmanageably as when the specimen is magnified 500 X.

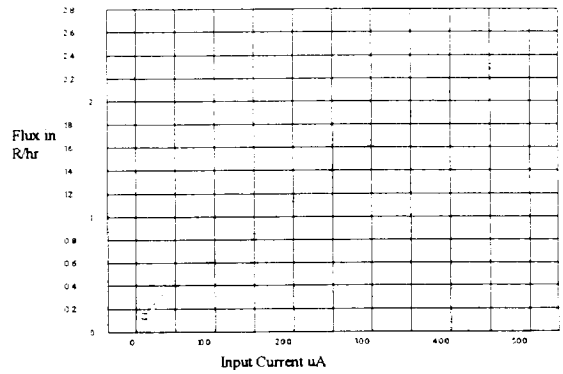

Figure 6. Measured flux vs. input current at 30 kV.

A measure of the flux vs. input current was made for 10-100 kV using the ionization survey meter. The plot shown in Fig. 6 shows the expected linear dependence of output with current shown here for the 30 kV range.

3.2 X-Ray Spectrum Measurement

One important aspect for modeling the specimen response to X-rays was the knowledge of the emission spectrum from the X-ray source. This information was not available from the manufacturer. (It is reasonable to not expect such detailed information for such a device when performance for the intended nondestructive testing applications don't require it.) However, accurate utilization of the X-ray transmission models developed in the first year of this ATD benefit from this data. The models prepared earlier in this work and discussed later, used published spectra for more common X-ray sources using a tungsten target.

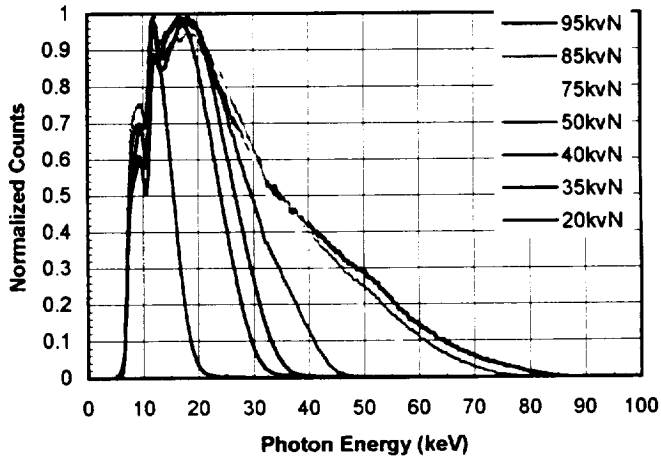

Figure 7. Normalized X-ray spectra from the Fein Focus High Definition X-ray tube.

It was reasonable to expect similar response from any tungsten target illuminated with high energy electrons.

To obtain our X-ray source spectra, a multichannel analyzer and room temperature X-ray detectors of Cd-Zn from EEG was borrowed from the CMMR at UAH to perform the measurements. The test data revealed that the fluxes emanating from the tube even at minimal operating current were swamping the detector. With care, the X-ray source was detuned to produce a low enough flux to produce the characteristic spectrum. The useful range of the detector is between 14 keV and 200 keV. This was adequate for our work. A set of spectra were obtained without concern to flux level since the overall shape of the curve was all-important. It was not expected that the spectra would differ from the published curves to the degree they did. The overall difference was in the peak energy for the given acceleration energy. In all cases, the real peaks were shifted to lower energies than the general published data.. In addition, the higher energy characteristic peaks often seen for tungsten were not found. The measured spectra for our micro-focus X-ray source are shown in Figure 7.

3.3 Absorption Model Calculations Performed

A first principles approach to determining the useful contrast from a sample was initiated. Using standard materials data and published X-ray spectra, the degree of absorption of the rays as they pass through the inhomogeneous sample was calculated. Resolution limits established by the converter / camera combination were introduced via MTF data for the X-ray image intensifier. This latter area of modeling will require much more work to be truly useful to predict which conditions and apparatus will be optimum. The effort to date does provide useful information about the likelihood of observing certain features and, to a degree, how high a contrast the feature may have under ideal conditions.

Source flux data for 100 kV acceleration and 50 kV acceleration were used. For all, a tungsten target, 1 mm Al filtration, and either a 10 to 100 keV or 10 to 50 keV spectrum range were used. These are conditions available from the from Fein Focus Microfocus X-ray source being purchased.

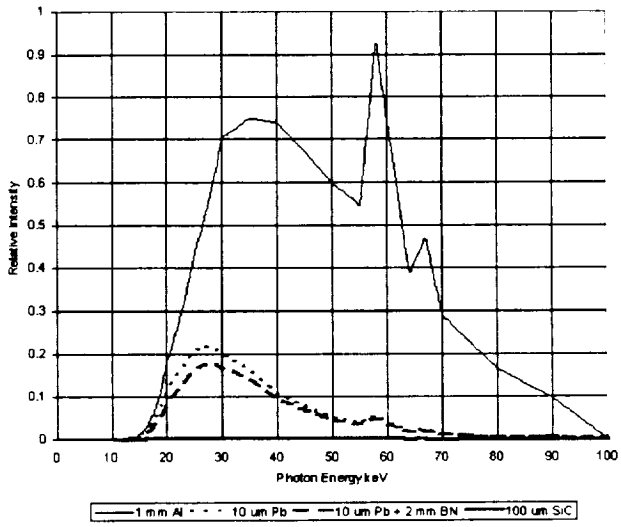

Figure 8. Difference flux spectra for 100 kV acceleration.

Absorption cross-section and density data over the range 10-100 keV were obtained for Al (solid and liquid), Pb, In, B, N, Si and C elements. For compounds like SiC and BN, one must first calculate mass attenuation coefficients from the elemental data and density data. The critical calculation for the absorption model comes from applying Beer's Law to obtain transmitted flux of different specimens.

The following specimen configurations were used in this analysis:

1 mm thick Al (basic specimen)
2 & 5 mm BN (crucible walls) with 1 mm Al
1,2,3,5 and 10 μm Pb, Bi, Au or In particles in the 1 mm Al
100 and 500 μm SiC and ZrO_2 particles in Al
10 and 100 μm voids in 1 mm Al

Intensity differences (for example between Al and Al with a Pb particle) were used to obtain image contrast data as a function of photon energy from 10-100 keV. Figure 8, below displays the different calculated spectra of transmitted photons through the specimen. The blue curve shows the transmitted spectrum of a 100 kV accelerated X-ray beam after passing through 1 mm of Al, where the raw beam's peak was normalized. The two lower curves show the overall flux of an Al specimen with a 10 μm Pb particle in it and with a crucible. The almost nil attenuation of a 100 μm SiC particle is shown in red at the bottom. These spectra describe the contrast information the particles provide.

Table I. Model Results for Various Configurations

Configuration (at room temperature)	Peak Contrast (out of 1)	Loss % (10-100keV)
1 mm Al vs. nothing	0.36	19.87
1 mm solid vs 1 mm liquid Al @ melting temperature	0.02	1.42
1 mm Al + 2 mm BN vs. nothing	0.46	30.7
2 mm BN on 1 mm Al	0.12	13.52
10 μm Pb in 1mm Al	0.21	15.5
10 μm Pb in 1mm Al + 2 mm BN	0.18	14.91
10 μm Pb in 1mm Al + 2 mm BN vs. nothing	0.62	41.04
10 μm In in 1mm Al	0.17	12.73
100 μm SiC in 1mm Al	0.0027	0.231
10 μm void in 1mm Al	0.0025	-0.19
100 μm void in 1mm Al	0.027	-1.94
		(10-50keV)
1 mm Al vs. nothing	0.44	36.9
1 mm solid vs 1 mm liquid Al @ the melting temperature	0.025	2.93
2 mm BN on 1 mm Al	0.12	17.5
10 μm Pb in 1mm Al	0.26	31
10 μm In in 1mm Al	0.18	17.8
100 μm SiC in 1mm Al	0.0035	0.43
10 μm void in 1mm Al	0.0033	-0.4
100 μm void in 1mm Al	0.033	-4

Contrast from the features in the specimen depends on several things. The major factors being the materials and the X-ray energy spectrum. One finds contrast varies from very little to considerable depending on the energy selected. Lower energies usually offer greater contrast. Secondly, the acceleration voltage produces X-rays from the tungsten target which have a peak output at 40% in keV photons, approximately, of the maximum acceleration voltage in kV. This however, is more of a flux issue and therefore can be compensated with exposure times. Since the X-ray image intensifier responds best to a range of photon energy (over 25 keV), the image contrast from this device is calculable as the integrated transmission over the full range of the photon spectrum used. This is better than the piecewise selection of absorption values at different parts of the spectrum. The latter shows what accelerations may be best to use or what filters to use (if they were employed).

The results from this model have been summarized in the table. Contrast of 0.01 or 1% is an target goal for observation. The NDT industry uses 2% as a minimum detectable contrast, but this is with film radiography.

This table shows sets of calculations for two energy ranges, up to 100 and up to 50 keV. Notice that lower acceleration can offer higher contrast as already proven with the experiments of the feasibility study. In the study, acceleration voltages of 35 kV were selected as optimum. However, as voltage goes down, so too does the overall flux for a given current.

X-ray Intensifier Resolution and Contrast Model Calculations

Contrast vs. photon energy data was obtained from the absorption model. Then the known MTF function for the Thompson CSF X-ray Image Intensifier was applied. If the initial contrast is low, then after conversion through the intensifier, contrast will be much lower if the features are small at the front end of the device.

It should be noted that the MTF calculation doesn't address the sensitivity of the intensifier. The intensifier only sees photons of higher energy than 25 to 30 keV. As a result, the high contrast peak of the curves occur at the energy the detector is least sensitive to.

For comparison, it is worth noting that the Non Destructive Testing (NDT) radiographic industry uses 2% minimum contrast for its detection criterion which is based on film radiography. If possible, then, we can adopt a 2% criterion and determine a resolution limit for the lower contrast from the MTF response. Unfortunately, the contrast from SiC particles in Al is so poor that we cannot expect to see the particles even when the particles are 0.1 mm in size. These calculations warrant the effort to coat dense metallic particles with SiC for future studies.

Mathematical Modeling and Solute Gradient Measurements

The X-ray absorption model needed to be examined more closely when it was observed that the calculated absorption level of silver was comparable to that of lead for equal thicknesses. To predict particle contrast, a 10 μm layer of the particle material on 1 mm Al is assumed and compared to 1 mm Al. The calculations unexpectedly showed similar absorption from these two elements. Closer examination showed that the molar density of the material plays a role in the absorption calculation in a way that alters the weighting of the atomic absorption. The

unexpected outcome of this analysis is that the selection process for the alloying elements is more complex than first thought.

The models cannot account for absorption when the elements are in solution unless the molar density is known. As a result, solutal measurements will be needed that support future prediction of solutal concentrations obtained from theories.

We have a strong desire to quantify the solutal gradients in the liquid ahead of the interface since this is a powerful tool in furthering the fundamental understanding of the solidification process. No one, to our knowledge, has a better means of measuring these concentrations. As a result, these details of absorption modeling are needed to best quantify the solute concentration measurements. To further this goal, it has been determined that a mechanism to measure absorption of a calibrated standard will need to be accommodated in the furnace design. This is because the measurement of solute concentration amounts to a measure of signal subtractions where there is normally no absolute reference point. The calibration standard will provide this reference.

3.4 Custom Manufacture of Suitable X-ray Resolution Gauges

An accurate resolution X-ray test target for feature sizes 1 μm or less is essential for comparative tests of the candidate instrument configurations. Custom ion milled gold and nickel resolution targets were procured and evaluated. Three such gauges were delivered and each evaluated with various microscopies to verify quality and calibration. Each of the three differ slightly but all provide the limiting resolution data. A search of the few companies in this country that could perform the task resulted in these items for our exclusive needs. The targets are glass plates with about 3 micrometers of metallization into which a standard pattern (USAF test target) was etched by ion milling. It is technically difficult to produce fine features that preserve the feature shape throughout a thickness that is greater than the width of the feature and especially to do so with heavy metals like gold. The pattern provides increasing line pair resolution to the limit of the X-ray source which is our tests show is better than 2 micrometer resolution of line pairs.. The gauge permits measure of the resolution and calibration of the instrument before use. These measurements have shown that adjustment and calibration of our microfocus X-ray source is frequently required (nearly daily) to maintain the ultra-high definition capability of this instrument.

4.0 Development of an Optimized Furnace for Solidification Studies

4.1 Furnace Development Summary

Extensive testing utilizing a prototype furnace has enabled us to establish the specifications for the second generation transparent (to) X-ray furnace. We ended up with the 4th generation furnace meeting our criteria. The prototype furnace (gen 1, built at UAH before this NASA ATD) enabled a maximum real-time magnification of the solidifying sample of about 35 X. In order to obtain real-time images of the growth of fine microstructural features (such as the fibers in eutectics and monotectics) we require a magnification of the order of 150 X. The primary difficulty is the requirement to place the molten metal sample safely within a few millimeters from the X-ray source without overheating the source. A higher magnification also produces a higher image quality at the converter/camera such that faint objects can be seen. The inherently high MTFs of the CCD X-ray cameras offer an advantage to this problem, but it will not go away completely regardless of what technology is used. Therefore, good furnace design is nearly as important to getting the best images as is the detector technology.

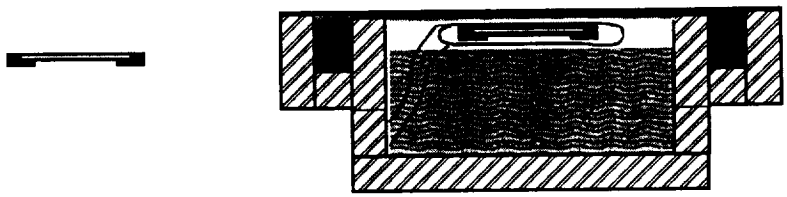

Figure 9. Cross section schematic of X-ray furnace (gen 2) on right showing water manifold on the sides and the heating element around crucible and separately, the specimen in crucible on left.

To safely bring a 1200 ° C heating element within a few millimeters of a temperature-sensitive mechanism is a very difficult task and it was one that took 2 years to solve. There is no form of insulation that adequately protects in such thin gaps. It was decided to use flowing, chilled water to protect the outside of the furnace. This can be seen in Figure 9 which shows the gen 2 furnace heater and the housing used in the gen 4 furnace. The upper, critical surface of the furnace is one millimeter thick and made from a copper alloy foil water jacket. The penalty of this approach is that the heating element must now heat the water as well as the sample. Both thermal radiation and conduction are the modes of heat transport at these temperatures. The remainder of the gap between the specimen crucible and the outside of the furnace is a high-alumina fibrous ceramic insulation capable of withstanding continuous contact to the heating element in air. Details of the materials selection and geometry were the most time consuming tasks. The new furnace can allow only one fifth the space for insulation compared to the prototype furnace. The upper wall of the furnace was designed to offer a uniform thermal field over the whole heating element surface. The tests of the gen 2 furnace, Figure 9 above, showed that (with one heating element and no specimen or crucible) the crucible space could reach 1200 °C and the power to the heater was 1 kW. For this condition, the outer surface of the furnace top was never over 45 °C and the water leaving the furnace was taking 500 W of heat with it. When a specimen was added, the interface could never reach the X-ray window and instead, 660 °C, the s/l interface temperature, was reached within the element itself even at 1 kW power in. The high heat loss through the specimen and crucible proved a second (already planned for) heater was needed on the 'cold' end to reduce losses from this end. After a second heater was added and the tests restarted, the gen 2 furnace failed at the solder joints

within the top assembly caused by thermal and mechanical stress cycling and corrosion. The thin walls (0.005 inch thick phosphor bronze) flexed from the water pressure and the solder joints (which were found not to be the best) failed over time. The heaters consumed a lot of power and it was not possible to position the interface of pure Al centered on the window (where there could be no heating or insulation). It was clear that the 'flat' furnace core design was not good for the size of specimen and proximity of the jacket.

Testing showed the above concept design did indeed work as expected. Calculations of temperatures within the walls of the furnace for the geometry and water flow conditions showed that a cessation of flow would cause the water to reach boiling temperatures in about one second. Experiments where flow was restricted and stopped showed that indeed these calculations were right. Adequate flow, pressure and uniformity of flow rate of the cooling water were all important for the furnace to work properly. During testing, the ribs of copper wire that joined the upper to the lower wall of the furnace top (water jacket) served as high heat flux sources and the outer wall temperature was significantly warmer over these ribs. These ribs were spaced one inch apart and they extended only over the narrow thickness of the jacket.

A redesign was prompted by these events to improve the furnace top structure. The basic design concept (gen 2) was retained which allowed the majority of the furnace to be retained. A new water jacket structure was constructed, but one that required more complex machining. From the experiments, it was determined that uniformity of thermal conditions over the top of the furnace did not influence the quality of the interface to the degree estimated. Since only a one inch window for the X-ray was needed, clearance for the X-ray tube was only needed for the mid third of the foot-long furnace. The other two thirds of the top could be made from heavier brass plates that will not flex and can have the ribs machined into their lower surface. The uniformity of the ribs, increasing their length and decreasing their spacing to 0.5 in. prevented water leaks and flexing under pressure. Flexing from thermal expansion cannot be eliminated, but the increased number of ribs helps resist failure. The 4th generation furnace is shown in Figure 10 and shows the external features mentioned.

Some problems in the first design were caused by the assembly method of having to solder all surfaces in one heating operation that required a jig and not being able to verify all joints since they were hidden. Special Teflon spacers had to be fabricated to keep the two walls of the water jacket from warping or contacting one another during the assembly process. The spacers had to be in place during soldering and then removed after cooling to open up the passages. This assembly method was done away with in the present design. The lower 0.005 in copper sheet that comes closest to the heating elements, was be soldered in place on its frame first. To further strengthen the assembly, this sheet is now made from Be-Cu alloy which is twice as strong as the phosphor bronze originally used. Contacting surfaces to the upper wall were tinned before the top was assembled. Before the top was added, the lower sheet was checked for a good seal. The upper wall was made from three pieces, with the middle piece being a brass sheet machined with ribs and a window seal such that the contiguous portion of this plate is less than 0.009 in thick. By placing a solid aluminum block within the furnace frame during soldering, the lower copper sheet was pressed against the ribs machined into the three pieces of the upper wall of the jacket. Uniform cooling of this assembly resulted in a better sealed and bonded structure.

There is a direct trade off in furnace design between maximum magnification and melting temperature. Our scientific research with the XTM has shown that an excellent range of fundamental solidification phenomena unobservable by other methods can be studied using

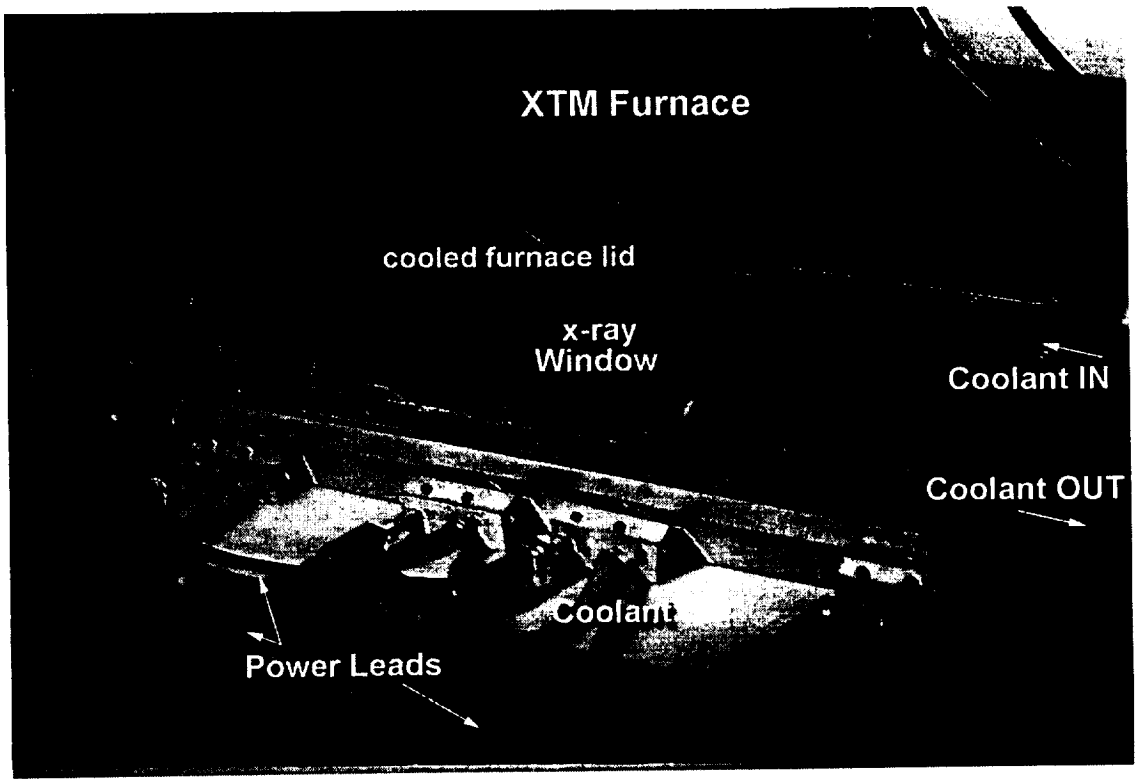

Figure 10. schematic of 12 inch long (gen 4) X-ray furnace showing middle window area to accept X-ray tube/source.

aluminum alloys. The added advantages of aluminum alloys are the low melting temperature (660 C) and the commercial interest in such alloys. From the fundamental solidification science perspective, the need for higher real-time magnification is quite evident. This drives the priority for furnace design to offer the highest magnification for these alloys so that the smallest solidification structures possible can be observed and measured. To address the science payback, this furnace design was be optimized for aluminum alloys where the heater elements need only to provide 1000 °C temperatures to the hot end of the specimen.

It was also desired to not require vacuum operation. So provision is made for inert gas operation by bleeding it through the housing volume.

It was planned to replace the Chromel heating ribbons with the boron nitride coated graphite elements to permit higher temperatures to be reached. This step would have required addition of inert gas flow and refurbishing the interior of the furnace for these 120 V AC devices. This arrangement could allow for operation up to 1200 °C. However, these custom heating elements arrived in a heavily bowed condition as a result of the process of manufacturing them. This was not expected nor correctable for the geometry of heater needed. The solution would have been to assemble a straightening framework made out of BN, that was strong enough to straighten the heaters to a flat configuration to allow the specimen in its crucible, to slide between the heater pairs. The structure would interfere with the cooled lid of the furnace and the specimen to X-ray source distance increased.

The main thrust of the work in this project was to achieve the best images of the structures. Higher temperatures were not a requirement to meet this goal since examples of most microstructures could be found in the aluminum alloys. So, instead, development proceeded to

make the high magnification, high resolution furnace design. One rule of thumb came out of this set of furnace designs (that influenced the direction of the design effort to the one with the best results): *Due to the constraints of proximity and temperature to the X-ray source (tube), in order to achieve high temperatures at high magnifications (short distances from the tube) the heated volume needs to be reduced as the magnification and specimen temperatures go up.* The high temperature aspect was temporarily shelved.

The furnace lid was indeed better than in gen 2, but the heater core assembly required major redesign. The gen 3 furnace consisted of a new heater core design with the recently rebuilt furnace lid. The heater core was reduced in cross section to use specimen crucibles, still of BN, having only a 5x5 mm cross section. Instead of running the crucible inside the heater winding, which would have provided a more efficient thermal coupling to the specimen, the crucible was to sit on top of the heater core which was made from machinable alumina ceramic. The heater element itself was to be Kanthal ribbon. Specimen heating was to be ostensibly from below. Ceramic webs or fingers extended the heated volume to the sides of the crucible. Figure 11 shows this design of this heater core. Testing of this heater resulted in similar results to the gen 1 heater core even without the use of the furnace lid. Heat losses overpowered the heat gain to the

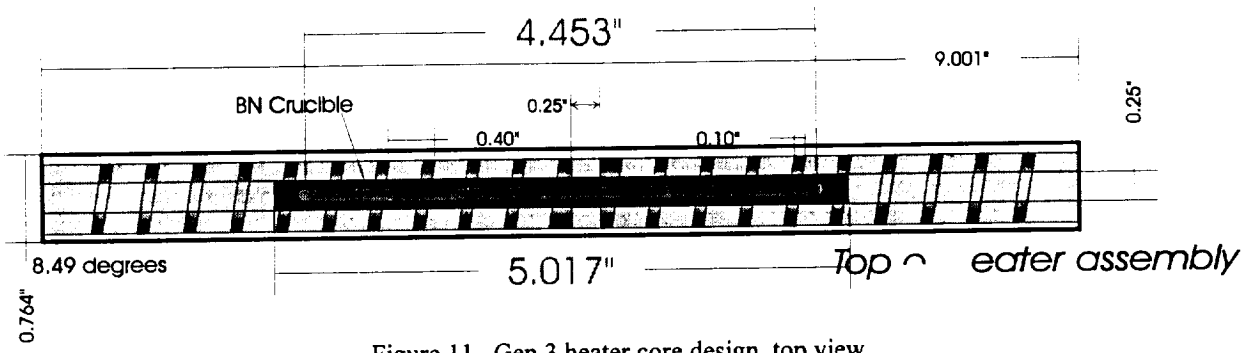

Figure 11. Gen 3 heater core design, top view.

specimen. The heat from the heater elements did not reach the central, unheated portion adequately, whether there was a specimen or not. The specimen needed efficient coupling of the heat yet still provide a free, unheated, unencumbered space for viewing without giving up a lot of heat to the furnace lid. This heater did not provide this.

4.2 4th Generation Furnace

Experiences with the first furnace designs have lead to new furnace that offers higher magnification and is safe. In this design, magnification is emphasized. Experience from years of work with organic model materials and furnace design established the concepts for the earlier furnaces. The earlier designs were based on wide, flat specimens to provide a uniform region of the solid-liquid interface to examine and present enough interface to scan for interesting features since some features along the interface image better than others. Since large expanses of interface cannot be viewed at high magnification, the specimen width need only be in the order of a few millimeters. With this stipulation, the specimen and crucible were to be pencil-like. The thickness can be 0.5 to 1 mm as usual. The small width offers high aspect ratio specimens that only have 25 to 50 mm overall length. Experience with BN crucibles shows that wall effects on interface planarity are minimal and so there should be few artifacts from the crucible.

The power required to melt the smaller specimen will be lower. The 4th generation furnace uses Kanthal A-1 ribbon heating ribbon.

From the above discussion, it became clear to properly heat the specimen, it should be actively heated on three sides and only allow the top to be exposed. For control purposes, the heated volume should be as large as possible for the thermal mass and stability. Placing the heater windings as close as possible to the specimen was the best approach. As seen in Figure 12, the specimen rests in a U-shaped depression formed in the winding. The mandrel, a slotted alumina tube, adds mass to the heater, retains the winding shape and aligns the two windings. The heater core was well insulated on all three sides with rigid, tight-fitting Zircar so only some heat is lost to the top surface and through the power leads. Figure 13 shows the mandrel and sample in an exploded view. Two ribbons of heater were spiral wound at each end of the mandrel leaving a 20 mm gap between them in the center. A window was cut in the alumina to pass the X-ray beam through this gap. During winding, the element was pressed with a form into the hollow of the mandrel to form the re-entrant U-shaped heater. The windings were heated to orange heat with a spacer in place to 'set' the metal heater windings shape. Refractory cement filled the spaces between the mandrel and the windings to hold them in place.

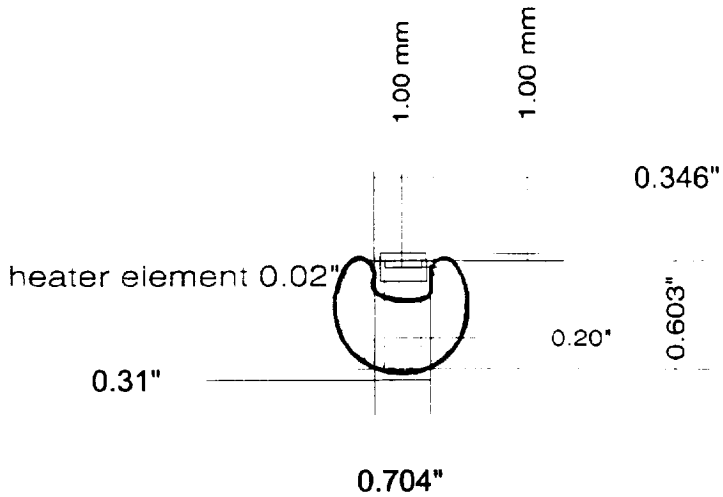

Figure 12. Cross section of Gen 4 furnace heater core showing proximity of the crucible and its sample to the heater winding.

The heat loss path between the heater winding to the furnace lid was minimized. This heater with the improved furnace lid now produces the temperatures needed and the magnification desired. On the 15" video monitor, through the intensifier and video camera, the magnification of a specimen in this furnace can be as high as 140X (with the tube pressed against the furnace top. This was quite safe to do since the furnace outer temperature was always and everywhere less than 40 C. Recently, features in Al-Bi approaching 5 μm diameter were observed in real-time with this furnace.

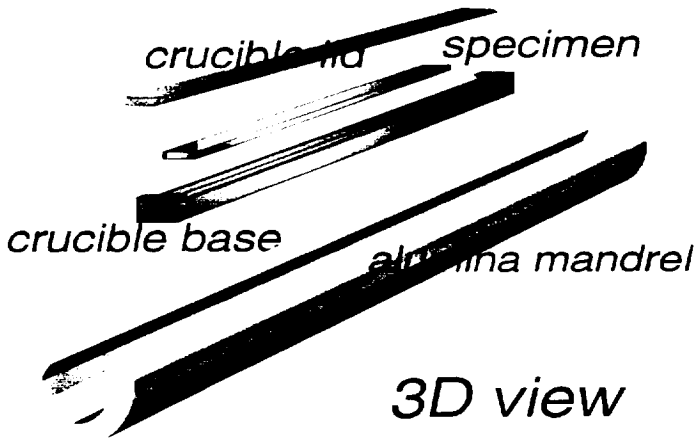

Figure 13. Alumina heater mandrel and BN crucible with lid and sample exploded view.

4.3 Translation Mechanism and Growth Rate Verification:

Solidification morphologies form with a large range of feature dimensions. It is possible to increase the feature size of fibers, lamellae, cells, dendrites and condensed phases, within limits, by using low solidification rates. Experience has shown that good results were obtained when growth rates were in the range of 1 μm/sec, which is a typical crystal growth rate. Solute additions cause interface breakdown at somewhat higher rates and dendrites form at about ten times this rate. Selection of rate and concentration of solute can be optimized to delineate the interface and its structures. To provide these low rates (0.005 μm/sec minimum) and still provide relatively high rates (10,000 μm/sec maximum), a 100,000 step per revolution Compumotor stepper motor was selected to drive a 50 tpi drive screw to translate the specimen in the furnace. Computer control of the motor offers significant benefits such as knowledge of the position, ability to repeat growth sequences, and the ability to vary the rate during growth. The nut on the screw is attached to a stainless steel rod that passes through the furnace wall and pulls the specimen into the cold end of the temperature gradient for solidification. See Figure 14.

The video data of one specimen was evaluated in detail for the Al-Pb TMS paper. Besides mounting and polishing this specimen for the successful electron microprobe work, low magnification film radiographs were prepared to show striations throughout the specimen volume. Furthermore, to avoid criticism that experimental conditions caused the striations, an analysis was performed from the video of the specimen interface velocity and translation velocity. This was prompted from analysis of the film radiographs that showed more growth occurred for the translation rate imposed. Interface motion exceeded the translation rate by as much as 35% due to the single heater furnace design.

Once the video was played back to take measurements, it was found that translation velocity and growth velocities were quite linear at steady state. During the initial growth transient, the growth rate was below the translation rate. But, for any translation rate, the measured growth rate was higher. From the measured growth rates, new growth distances were calculated and found to correlate well with the specimen post-growth evaluation. This prevents the criticism that periodic translation (meaning growth) rate fluctuations could account for the striation formation. Furthermore, the XTM can be used to monitor true growth rates.

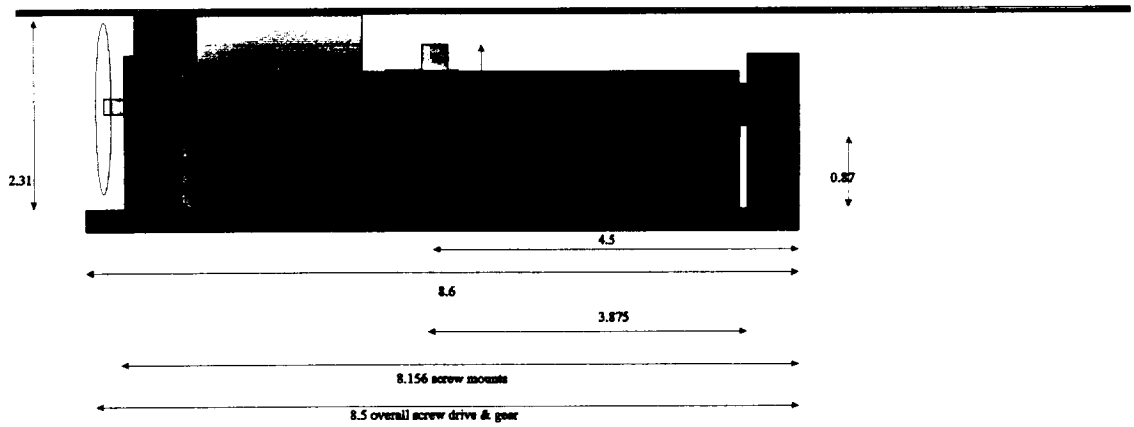

Figure 14. Side view of translation mechanism and furnace. Translation mechanism consists of stepper motor, screw drive and push/pull rod.

5.0 Optimization of X-Ray Converter/Camera for Solidification Studies:

A critical component of the development of the solidification XTM is the detection of the X-rays and their conversion to a useful image. Five technologies all based on CCDs were evaluated for the X-ray camera/converter. Their performance was compared to film and other converter methods. Although some aspects of these technologies are a few years old, the selection of one as the best for this application could not be made based on specifications or claimed performance. The oldest technology was the X-ray image intensifier for image conversion. This equipment was coupled with the cooled CCD camera and permitted the extraction of the best images possible from the technology. The intensifier is now used with a low-noise Dage DC 3000 3-CCD color video camera. Three technologies are based on intimate coupling of the converter and CCD itself. In fact, one promising method uses the CCD silicon itself as the X-ray to electron converter or detector. Two technologies puts a scintillator in front of the CCD and converts the X-ray photons to visible light photons that the CCD can convert to electrons and store in the pixel elements until time to read out the pixel charge.

The fifth, and promising technology addresses the improvement in intensifier design and in CCD utilization. This device combines both in one sensor and is known as the Electron Bombarded CCD. Comparisons between the technologies have shown that a balance between contrast, resolution, signal to noise ratio, and sensitivity must carefully be examined. This sensor was 'designed' and ordered during the second year of this contract, but has not been delivered to date. It's evaluation cannot be included in this report.

Thus we have conducted a careful test program on several candidate X-ray detector technologies and made the necessary evaluations.

5.1 X-ray image conversion methods

A critical component of the development of the solidification XTM is the detection of the X-rays and conversion to a useful image. As is often the case, there is no *best* technology. The oldest technology (invented 1950s) is the X-ray image intensifier for image conversion. On coupling this device with the cooled CCD camera, the best images possible using an intensifier tube were obtained. However, signal gain is traded for resolution. The other four technologies are based on intimate coupling of a scintillator (X-ray image converter) and the CCD itself. Fig. 15 shows the direct conversion X-ray CCD camera used for the testing. The remaining three approaches put a scintillator in front of a CCD to convert the X-ray photons to visible light photons. These in turn are converted to electrons and stored in the pixel elements for later read-out. In the fifth technology addressed here, the scintillator image is converted to an electron image by a photocathode. By impressing a high electric field between this photocathode and a nearby CCD, the electrons are accelerated into the CCD where they are collected (thus the name electron-bombarded CCD or EBCCD). In this way, some gain is obtained. These four CCD based sensors have an insignificant limitation - a limited field of view or a small area. Our work is concerned with object fields smaller than the sensor which were magnified by the XTM.

CCD technology is well established. CCDs have a high detection efficiency (DQE or detector quantum efficiency) with visible light wavelengths. They provide the numerous benefits for digital image processing and offer real-time tracking of dynamic processes (such as

solidification phenomena). The issues of contrast, resolution, signal to noise ratio, and sensitivity must simultaneously be examined.

Figures 16a-18a collect the schematic diagrams for the EEV CCD sensors evaluated in this work. They are the direct conversion CCD, the scintillator deposited on the CCD and the scintillator deposited on a fiberoptic faceplate bonded to the CCD. Arriving from the top in each diagram, is an X-ray photon which is absorbed in the converter layer. Figure 16b-18b is set of corresponding resolution test images from the sensors.

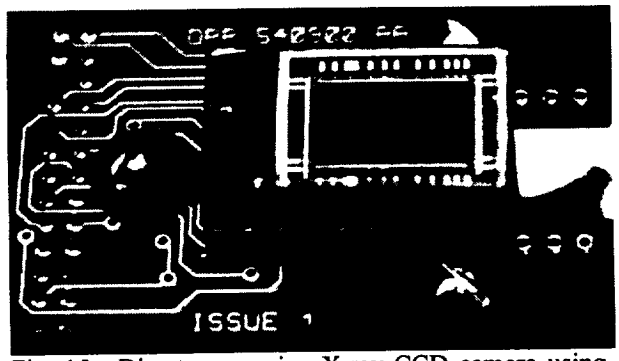

Fig. 15. Direct conversion X-ray CCD camera using EEV CCD02-06-5-207 sensor.

The direct CCD converter became available several years ago. This technology uses the silicon in the CCD as the X-ray photon converter and as the photo-electron storage device so it can be displayed after read-out. Acquisition times and dynamic range are increased by cooling the CCD to about -25 ° C. One limitation is the low number of X-ray photons detectable before the sensor is saturated. Another limitation is the low stopping power of Si to hard X-rays. Resolution and MTF on the other hand are superior. When enough flux is available, the low DQE or detection efficiency is less of an issue.

The second and third technologies use a cooled CCD as a sensor for the *visible* light image from a scintillation screen which converts the X-rays to visible light. Low detection sensitivity is again a difficulty. Resolution and contrast are not a significant problem. The scintillator, for example CsI, is placed directly on the CCD surface, Fig. 17, or deposited onto a fiberoptic face plate which was optically bonded to the face of the CCD, Fig. 18. One of each style of CCD was obtained as engineering grade (having a few known faults) from EEV in England. These were 0.85 x 1.2 cm devices (model CCD 02-06) with 578 x 385 pixels of 22 μm size. Cooling the CCD was not a requirement for this evaluation so only 8-bit images were obtained.

The EBCCD is the most promising imaging technology to date. However, the device

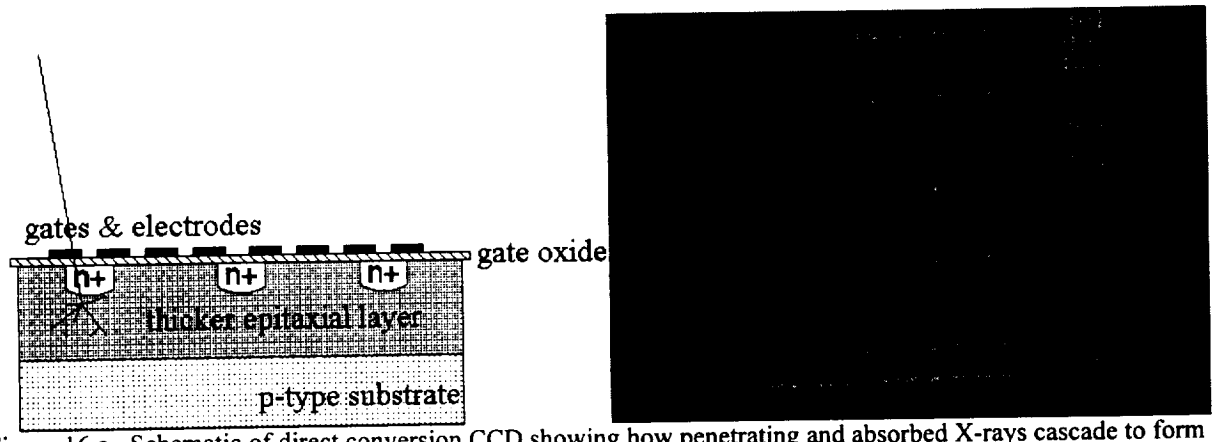

Figure 16 a. Schematic of direct conversion CCD showing how penetrating and absorbed X-rays cascade to form free electrons in the Si. 16 b. Resolution test image of the EEV direct conversion, deep depleted CCD showing excellent sharpness.

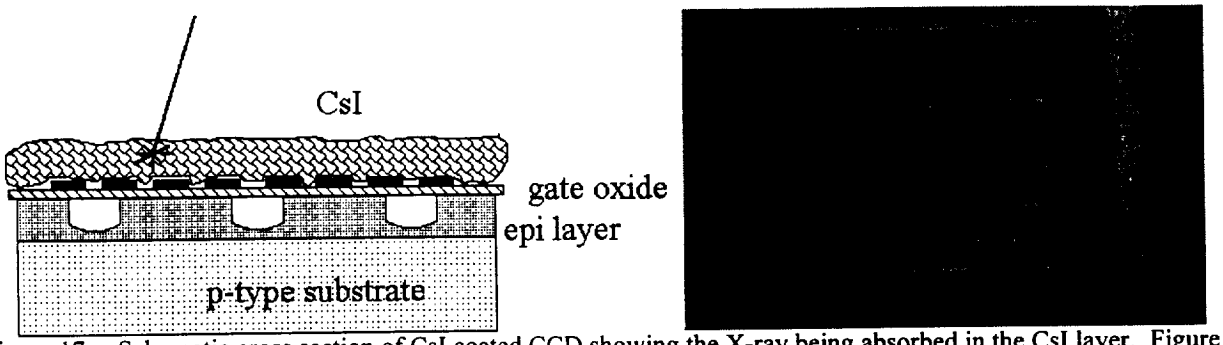

Figure 17 a. Schematic cross section of CsI coated CCD showing the X-ray being absorbed in the CsI layer. Figure 17 b. Resolution test image showing considerably less sharpness than the direct conversion CCD. Light generated within the scintillator can be diffused by the scintillator to neighboring pixels.

does not yet exist as an X-ray camera. Similar devices do exist, Fig. 19, as visible light cameras and the performance can be predicted. More will be discussed later.

Other sensor configurations have been evaluated and found less worthwhile for XTM use as it is presently configured. If the X-ray energies employed for XTM were raised to 100 keV and higher (to MeV), then a fiberoptic faceplate made from glass scintillator material would be a prime candidate. Scatter of the image is reduced by the fiberoptic structure and the absorption is determined by the thickness of the faceplate. Bonding the faceplate to a CCD directly can give very good results.

Intensification of a scintillator screen can be obtained using night-vision technology employing a microchannel plate proximity focused to the photocathode and the output phosphor. Small X-ray intensifiers (ICCD) like this are available but have seen limited commercial use because of their small size. This would otherwise not be a problem here, except these devices have high gain and high noise. The dynamic range is limited to 10 bits and the MTF of the device is reduced by the multiple scattering interfaces. They are however, superior devices compared to the intensifier tube. Of course radiographic film can be used when real-time or motion requirements allow. The ultimate resolutions are possible with film. Sensitivity is low and varies with the thickness of the silver-bearing emulsion, with X-ray films often having double layers. The DQE of film (see Table II) is so slow that long exposures (minutes) are needed. Greater density of the image increases the contrast such that in industry, to see the low

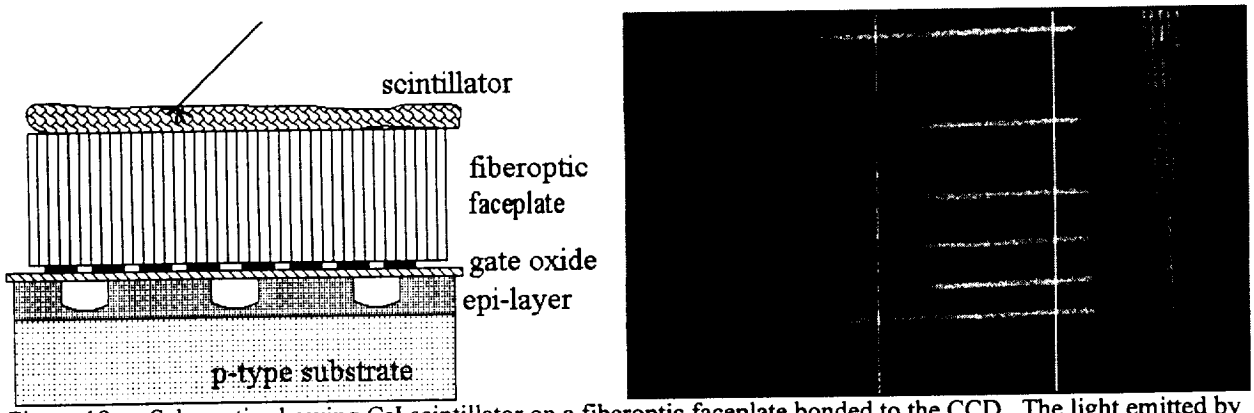

Figure 18 a. Schematic showing CsI scintillator on a fiberoptic faceplate bonded to the CCD. The light emitted by the CsI is sent straight to the CCD pixels by the fibers under which the event occurred. Fig 18 b. The resolution test image of this sensor shows better resolution than the CsI on the CCD and formed a brighter image than the direct conversion CCD with some loss of sharpness.

contrast features, the film is exposed to black image with density level of 2 or more.

5.2 Progress in Evaluation of X-ray Intensifier Technology for X-ray Conversion.

The science return of our recent solidification experiments with aluminum alloys of various kinds has been limited (as anticipated in our proposal) by the X-ray intensifier technology. The limitation is most apparent when attempting to observe the finest microstructures. The best science return is achieved consistently when the magnification is as high as possible, the flux is as high as possible and the acceleration voltage of the X-ray source is above 50 kV. No images can be obtained below 30 keV because that is the lower cutoff of the intensifier. Presently, we are using the state of the art X-ray image intensifier from Thompson CSF which was purchased with the Fein Focus Inc. apparatus. Coupled to this intensifier, we placed a cooled CCD camera having 1000x1300 pixels with 12 bits per pixel capability. This camera is a significant improvement to the uncooled CCD camera normally supplied which is much like those used for closed circuit TV. The uncooled camera cannot provide the image quality required for solidification studies but does offer movie-like video images. With higher contrast specimens like the Al-Ag alloys, interface morphology is viewable with the video camera. At best, such a camera only provides 256 gray levels as compared to the 4000 from the cooled CCD. This detector allows true real-time observation of the a moving sample (instead of exposures of several seconds required for the higher resolution cooled detector system). Scanning through the specimen in real-time where the image responds instantly as in regular television provides an extraordinary appreciation for the 3-D phase structure of the sample. Microstructural detail and spatial relationships are instantly appreciated. A sense of depth is perceived (due to the parallax effect) when laterally scanning where the different strata within the specimen shift at differing speeds. The state of the art optimized converter/camera may allow both the highest resolution and true real-time observation. However, the rapidity of the image rate will depend on sensitivity, magnification and flux. Certain conditions may not offer smooth movie-like image rates with the new camera.

Our initial configuration of the XTM uses an intensifier tube of a tri-field type that permits higher magnification (zoom) through electronic means within the intensifier. The penalty here is the image is less bright, or in other words, the intensifier gain is cut proportionately, thus, only with high fluxes and stationary objects could these higher magnification factors be of benefit. There is a marginal improvement in contrast and no improvement in resolution (since the cathode coating is the limiting step). Our conclusion is that the tri-field capability is not optimum for real time solidification studies for microstructural features of smaller than about 100 μm.

The use of a CsI coated CCD (which itself is cooled to provide the best S/N ratio) which offers as many as 16 bits per pixel dynamic range. The CsI coating converts the X-rays to visible light which is directly coupled into the CCD. The coating should shield the CCD from X-rays and protect the CCD while minimizing spurious signals. However, thicker coatings increase absorption while decreasing resolution.

Adding the fiber-optic face plate allows the X-rays passing through the phosphor layer to be blocked by the glass faceplate before damaging the CCD. Then phosphor coating can be made as thin as required to provide adequate resolution.

The dynamic range desired depends on the number of X-ray photons detected. The direct conversion approach may not permit as many photons to be detected to give the desired dynamic range. This comes about from the large number of electrons created per absorbed X-ray photon (~300). Full well electron capacity of the pixel is set by its volume and is limited to about 500,000 for the devices we are interested in. The dynamic range is simply the number of detectable photons per pixel or 500,000/300 = 1666. This offers at best a range of 10 to 11 bits per pixel. The other methods using a scintillation layer offer up to 16 bits where an estimated 5 electrons would be created from each absorbed X-ray in the scintillator layer. This in turn means that more X-rays are needed to fill the well or to obtain the dynamic range desired.

Resolution from any of these CCD methods will be far superior to the image intensifier approach. However detection efficiency may determine the optimum technology, since our requirement is real time detection of solidification microstructures.

In the Electron Bombarded CCD (EBCCD) method from SiTE, the front half of the imaging sensor is like an image intensifier used for night vision devices. The second half replaces the conventional phosphor layer that converts electrons to visible light with a CCD that simply collects the electrons. A bi-alkali photocathode layer first converts photons to electrons. In the EBCCD, no intensification stage is added after the photocathode. The secret to the device is that the photocathode is (as it is called) proximally focused onto the CCD. This means that the photocathode plane is close to the CCD plane such that the electrons from the photocathode jump straight to the CCD with the help of an applied high voltage. Furthermore, the CCD is back-thinned and the electron collection surface is actually the rear of the CCD sensor. The elements are on the front face of the CCD that read out the charge collected at each pixel when needed. For signal to noise purposes, this device can be cooled to offer up to 16 bits per pixel. Proximal focused devices have existed for some time and offer high MTF and resolution. They also offer intensification that depends on the acceleration voltage used. In the EBCCD, intensification of the order of 100-200X is possible. This level of intensification is comparable to the intensifier we presently use.

Figure 19. EBCCD device (camera) for visible light without read-out electronics connected.

With intensification, exposure times should be lower. The devices at present offer quick readout times that approach video rates. However, the devices are not yet meant for X-ray use and only have 512x512 resolution at this time. We established the design and function criteria for such a device for X-ray use where a fiber-optic faceplate is used for the front window to support the photocathode. (This device is a high vacuum device.) On the front of the faceplate, another faceplate with a phosphor coating, e.g. CsI, will be added. The faceplate/phosphor combination will have to absorb the X-rays lest some get absorbed in the silicon of the CCD and create noise (like in the direct conversion CCD). The photocathode will be converting visible light from the phosphor to electrons. Some resolution loss will be caused there. However, the intensification possible will make this more of a real-time video device. The lower number of

pixels can be compensated for bringing the sensor closer to the specimen. The sensor is smaller than desired, but this is a first.

5.3 Tests with intraoral dental X-ray camera and microfocus X-ray source:

With the cooperation of Fein Focus USA, and General Imaging of Florida, we performed a performance evaluation with one of the prototype dental X-ray cameras in Atlanta. This device is commercially available for dental imaging applications and uses direct conversion in the CCD silicon. Because of its specialized use, limits to performance exist which need to be addressed with a similar unit used with the X-ray Transmission Microscope. The Fein Focus X-ray generator offered the X-ray beam conditions used during the feasibility study. The CCD device was exposed under comparable conditions to the aluminum alloy specimens during the earlier work.

Results show a high resolution (over 3X more than inherent resolution of X-ray image intensifier). In addition, of significant consequence, it was determined that the CCD was as sensitive as the X-ray image intensifier + camera combination that is presently the best performer. Due to the lack of available data from the manufacturer, such a determination would not have been possible from modeling or calculation determinations. Performing these hands-on evaluations is the most efficient way to show the proper course of action to take. It was also determined that the device was very small and easy to use. There is a potential to improve dynamic range to 14 bits by adding active cooling and better readout electronics, compared to 10 bit limitation for best X-ray image intensifiers.

Results were obtained from a couple of resolution tests and a real specimen of 1 mm thick aluminum 3% copper alloy that was previously processed during the feasibility study but never cut for analysis. The specimen in its boron nitride crucible was radiographed by placing it onto the CCD intraoral detector and irradiating them with a 35 kV beam to match the conditions obtained during the feasibility study. A two second exposure yielded almost identical results to the feasibility results where an intensifier and cooled CCD camera were employed. Resolution tests were performed using line pair gages which showed, with no net magnification, that the CCD intraoral detector could resolve 20 line pairs per millimeter. This is three times better than a unity magnification resolution with the X-ray image intensifier.

5.4 comparisons of five imaging technologies for X-Ray microscopy

X-ray image intensifier tube coupled to a cooled CCD camera

Our evaluation of X-ray imaging technologies refers to the capabilities of a conventional tube intensifier system. This is readily seen when comparing the MTF curves shown in Fig. 7 or the resolution data in Table 1. Two other curves in Fig. 7 are for CCD sensors and will be discussed later. It is known in the medical and NDT industry that such tubes are capable of 10 bit gray scale separation (60 dB S/N or 1000 levels). To extract this dynamic range, we substituted a cooled CCD camera (Photometrics Series 200 with full frame Kodak 1100x1300 sensor) for the 8 bit (256 gray levels) video CCD camera normally employed with these tubes. This camera offers a greater dynamic range (12 bits or 4096 gray levels) and resolution compared

to the uncooled CCD (interline transfer) camera normally used. Cooling the CCD prevents the accumulation of thermal electrons during the exposure. Reducing the noise level this way allows prolonged exposures when the intensifier efficiency is low. Using the cooled camera with the intensifier and 35 kV acceleration on the X-ray source, required exposures of 0.2 to 2 seconds were commonplace.

A regular, NTSC video (uncooled) CCD camera cannot provide the dynamic range we need for solidification studies but it does offer full motion video at 30 frames per second. With great care, a planar interface in 1 mm of pure Al be detected with an 8-bit camera in our XTM. Only 7 of 256 gray levels separate the liquid from the solid. Constitutionally undercooled cellular or dendritic structures cannot be seen with 8 bit cameras unless the solute is highly X-ray absorbing.

Testing CCD X-ray sensors

Each of the three EEV CCD devices was tested with the line-pair gauge (made of etched lead) placed on top of the sensor to provide a consistent input, Figure 16b-18b. Exposures were made with 50 kV and 350 μA at the source for 0.1 sec and the CCDs were 5 inches from the source covered by one layer of Al foil. Image quality allows one to rank the performance as direct conversion CCD, fiberoptic + CsI on CCD and last, CsI on CCD. The maximum resolution of this gauge is 22 line-pairs per mm and it was fully resolved in the direct conversion and fiberoptic devices implying they may have higher resolution.

The first of the CCD's we evaluated was the CsI coated CCD. Thicker coatings can absorb more X-rays and both increase capture efficiency (DQE) and better protect the CCD. However, thicker coatings decrease image spatial resolution (MTF). High noise levels can occur if X-rays transmitted through the coating are absorbed by the silicon in the CCD since many ($> 10^4$) electrons will be created from each single photon captured and brighten that pixel. It's desired that all X-rays be totally absorbed in the scintillator layer which implies that all photons are converted.

The next sensor added a fiberoptic faceplate to the CCD which is coated with CsI scintillator. Each fiber is a conduit of light on the 5-10 μm scale. The fiberoptic could have been tapered with a 2:1 or more ratio in front face diameter to rear face diameter. This latter arrangement has found use in X-ray crystallography and mammography applications. However, to reduce losses in the fiberoptic and because a large field of view is not required, the fiberoptic faceplate we employed is only 3 mm thick and has a 1:1 ratio. We can produce a thinner phosphor coating on the fiberoptic because the X-rays passing through the layer will be absorbed by the glass faceplate before damaging the CCD or adding noise. Thinner coatings improve resolution by reducing scatter within the coating. Coupling losses (phosphor to CCD) are increased but spurious signals from stray X-rays getting into the CCD elements is eliminated. It was decided to use a CsI coating on the faceplate since it can be deposited in a thick layer of 100-120 microns while still retaining high resolution since the deposition structure is in the form of aligned needles so it acts like a fiberoptic itself.

The third sensor we tested is the X-ray hardened direct conversion CCD. Radiation damage would accumulate although at a much slower rate than in conventional CCD's. The CCD would need replacement every two years. Efficiency is favored at lower photon energies (<10 keV photons). Silicon has a low cross-section compared to the scintillator materials and so

will not stop as many X-rays above these energies thus providing less signal. To compensate for this, the absorption (epitaxial or epi) layer is thickened from the typical 5 micrometers to 50 micrometers to capture more X-rays. The substrate is made from a high resistivity p-type Si. Still, less than 0.5% of 40 keV X-ray photons are absorbed in the sensor. This method offers the best resolution since little scattering is incurred within the CCD (compared to thick phosphor coatings). The direct conversion CCD technology offers a high MTF. The lower efficiency of detection and the low fluxes generated by the X-ray source at the low accelerations where this device works best made this CCD a secondary choice.

Earlier experiments with lens-coupled particulate Y_2O_2S-Eu phosphor coatings delivered only a 16 lp/mm resolution with ~30 μm layer thickness. This shows that the CsI scintillator is capable of better resolution while having a greater thickness (120 μm) of deposit. Intensity plots for each image revealed the relative sensitivity differences. The brightest image was obtained from the CsI coated CCD while the direct conversion was the least bright for equivalent exposures. Intuitively, the CsI on the CCD sensor should be superior, but the scintillator fills the gaps between the pixels and so adds noise by spilling light into adjacent pixels to reduce resolution. The fiberoptic faceplate constrains the light from the scintillator into small bundles and directs it to the pixels. Only glass fibers situated on a pixel element will illuminate it. The small loss of light is compensated by the improved resolution and protection of the CCD from X-rays.

Comparison between sensor configurations

These competitive technologies are not clearly delineated by performance. For example, one comparison using manufacturer's data can be made between CsI coated and direct conversion CCDs. The result is that the best S/N ratio available depends on the X-ray energies involved. Selected information regarding these sensors is collected in Table II.

Table II: comparison of converter/camera properties:

#	Description	Max. Resolution lp/mm	lp/mm @ 50% MTF	X-ray DQE
1	Thompson CSF 9" X-ray intensifier tube (TH9428HP)	4	1.4	65%
2	CsI on EEV CCD[a]	17	?	min 20%
3	CsI on FO on EEV CCD[a]	22+	?	min 25%
4	Direct Conversion CCD	22+[a]	15 [9]	10% @ 10 keV, 2%@ 35 keV
5	Pixel Vision EBCCD	25-30	30	min 20%[a]
6	Radiographic film	>100[a]	?	4% @ 70 keV

a based on measurements made in this work

The table shows the higher resolutions available from the alternates to the conventional X-ray tube. Although there is no standard, we found that the maximum resolution limits are often found at MTF values of 2%. The 50% MTF spatial frequency shows that contrast drops

significantly even for modest feature sizes. Accurate DQE values are difficult to obtain but are shown for comparison purposes. While it is always better to have a higher efficiency, the CCD sensors are small and can be placed closer to the X-ray source and therefore receive a higher flux. The intensifier tube has to be positioned (in our case 21 inches) far from the source to illuminate the large input window. The EBCCD offers gain which permits the sensor to placed farther from the source and so offer higher magnification without loss of resolution. The lower estimated DQE of the other CCD devices will require they be placed closer to the source to obtain a good signal. In spite of the low efficiency of the film, it is still the most common radiographic sensing method. The CCD sensors collected here all are competitive with film for resolution and offer the benefits of real-time imaging and digital recording.

Operation of the X-ray source with low energies offers higher contrast regardless of the detector. We found the optimum energy for aluminum alloy systems is 35 to 50 kV acceleration voltage with the intensifier tube. The thin specimens do not attenuate very highly and so low energy use is preferred. The dynamic range desired depends on the number of X-ray photons detected. The direct conversion approach will not permit as many photons to be detected to give the desired dynamic range. This comes about from the large number of electrons created per absorbed X-ray photon. One electron will be created for every 3.65 eV of the X-ray photon absorbed (about 11,000 for a 40 keV photon). Full-well electron capacity of the pixel is set by its volume and is limited to about 500,000 for the devices we are interested in. The dynamic range of the direct conversion CCD would simply be the number of detectable photons per pixel or 500,000/11,000 = 50. This offers at best a range of 4 bits per pixel. The other (scintillator) methods offer up to 12 bits where an estimated 200 electrons would be created from each absorbed X-ray in the scintillator layer. This in turn means that *more* X-rays are needed to fill the well i.e. to obtain the dynamic range desired.

Selection of 2 CCD technologies for the XTM

Based on the evaluation, two selections of CCD technology type and specifications for the optimum detection system for solidification studies was made. One is not intensified, and the other is.

The first selection was the scintillator/fiberoptic/CCD stack. The bid winner was Princeton Instruments Inc. The CCD has the largest number of pixels available (EEV CCD 05-30 with 1242 x 1152 pixels). A 3 mm thick fiberoptic faceplate is used and coated with CsI to a 100 μm thickness. The readout electronics purchased with the camera head permit as many as 16 bits (128,000) gray scale resolution per pixel and a 1 MHz clock rate at 14 bits per pixel. The CCD is thermoelectrically cooled to -30 °C and sealed in an air tight housing to obtain the optimum performance level and prevent condensation. A to D conversion is done in the camera and the images stored and subsequently enhanced in the computer. Figure 20 shows the device.

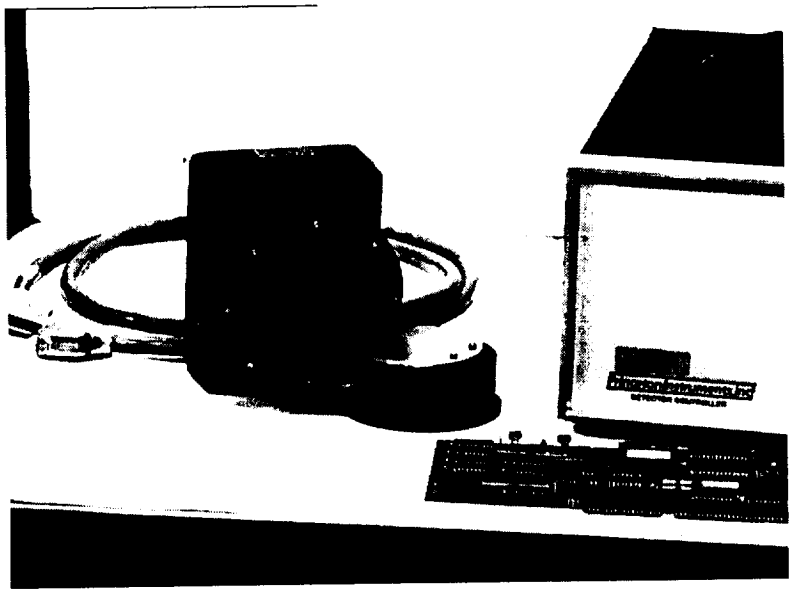

Figure 20. Princeton Instruments Inc. X-ray camera.

The second selection, which does not exist at this time, employs the electron bombarded CCD technology where a proximity focused photocathode is illuminated by a scintillator. The cooled, back-illuminated CCD would have 25 μm wide pixels in a 1024 x 1024 array. The sensor will be quite compact at 40 mm in diameter. The front window of the vacuum tube would be a fiberoptic faceplate and support a GaAs photocathode which is suited to the green emission of the CsI scintillator. The CCD in the sensor is made by SITe Inc. and the package and readout electronics produced by Pixel Vision Inc., a spin-off company from SITe specializing in low light level imaging CCD cameras. This camera represents more than the state of the art. A similar EBCCD sensor for low light level imaging was recently made commercial (Figure 19) after development by Pixel Vision Inc. and as a result, they were deemed the sole source for the device. Although perfectly suited for the XTM application, this device would benefit medicine for mammography and industry real-time radiographic NDT applications such as failure analysis or inspection of electronics. To date, although ordered, it has yet to be received.

images, which require two views of the sample, one for each eye, a special set of high definition electronically switched glasses were purchased to function in conjunction with the monitor. This stereo image viewing system is called Crystal Eyes and comes from a company specializing in such products. Now, stereo images can be viewed by 5 individuals simultaneously by each wearing the special glasses when looking at the computer monitor. The digital images obtained by taking two views of a specimen are displayed on the monitor in sequence such that each eye receives only one image. The glasses thereby ensure a left image goes in the left eye and the same for the right eye. The high performance of the system allows 1240 x 1024 pixel stereo images to be displayed without annoying flicker or misconvergence in a normally lighted room.

Other methods of stereo display were tried but the above system was found to be the best. The disadvantage is that stereo images cannot be distributed to other computers unless a similar capability or equipment is available.

Stereo pairs can be prepared from microradiographs as in the Figure 21 where relaxed vision permits merging the pictures into a stereo image. Structures like these benefit most from stereo imaging techniques.

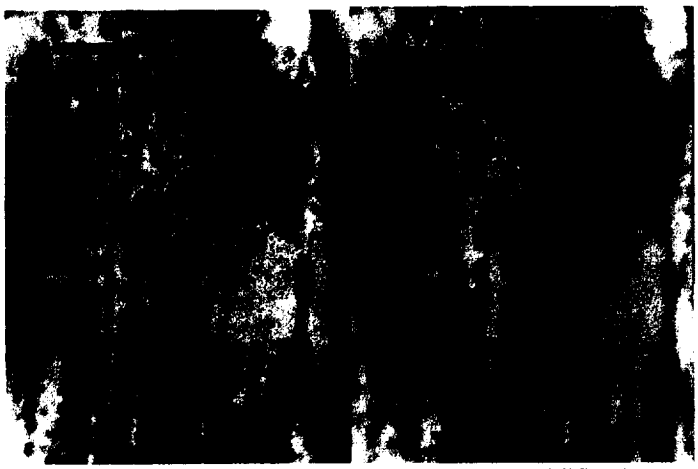

Figure 21 Stereo pair of Al-Bi monotectic post solidification. These images are high magnification views, post processing, dark particles are Bi.

6.0 Capabilities of XTM Real-time Solidification Studies

We have successfully imaged in real-time: various interfacial morphologies, nucleation, coalescence, incorporation of phases into the growing interface, particle pushing, and the solute boundary layer in the liquid at the solid-liquid interface. We have also measured true local growth rates and can evaluate segregation structures in the solid and perform metallographic measurements.

Results shown will be from the two furnace types, the prototype furnace, and the high mag-high resolution furnace (4^{th} gen). The figure captions outline the main features of each example.

To date, within the limits imposed by the *prototype* furnace, many of the solidification structures we originally set out to observe have been detected. In particular, the cellular structures caused by constitutional undercooling have been clearly seen in alloys having only a few percent of solute. The onset of the instability can also be observed in real-time. See Fig. 22, right side. Planar interfaces are normally ordinary in appearance but occasionally, under the XTM, interesting features like grain boundaries that intersect the solid-liquid interface can be found. See Fig. 22, left side. Losses in image quality incurred through printing conceal the darker band of solute found in the liquid against the solid in these Al-Ag alloys. However, the solute boundary layer is clearly seen in the monotectic alloys we have studied. This is shown in Fig. 23. The right part of the figure shows the optical density (absorption) profile along the line shown crossing the interface and the solute layer in the liquid.

Planar interfaces become a baseline structure for measurements of the perturbation of the interface shape when nearby a void or particle. Figure 24 shows two cases where the insulating particle perturbs the local interface shape due to the altered heat flow. Real-time observations showed the interface shape was different during growth than at stationary equilibrium. Sometimes, particles can be pushed by the s/l interface in a MMC as shown in Figure 25. Figure 26 shows two cases of the interface shape and the calculated shape when near a cylindrical hole. The predrilled hole produces the ideal experimental geometry to compare the calculated shapes to. Figure 27 shows the interface distortions caused by two voids that formed as a result of the coalescence of rejected gas impurities during solidification. Some of these voids become engulfed by the solid and attain an elongated shape.

Our XTM experiments verified the feasibility of observing pushing/engulfment by the solidification interface of spherical 30-70 μm zirconia particles in 5 mm aluminum matrix in near real time. Flight samples were examined before and after flight to make measurements of the pushing distances.

Examination of samples post solidification, when the magnification is not limited by the furnace structure, show even more structure and detail. The contrast improvement raises small-feature detectability above the noise floor. Some features, like the fibrous structures in the Al-Pb monotectic are so fine (about 5 micrometer diameter) that they could not be resolved in-situ using the prototype furnace. This is shown in Figure 28.

One significant discovery made with the XTM is the formation of striations in some monotectics. Figure 29 shows a low magnification radiomicrograph of an Al-Pb specimen. Only by integrating the absorption variations through the sample at the proper angle could these periodic structures be seen.

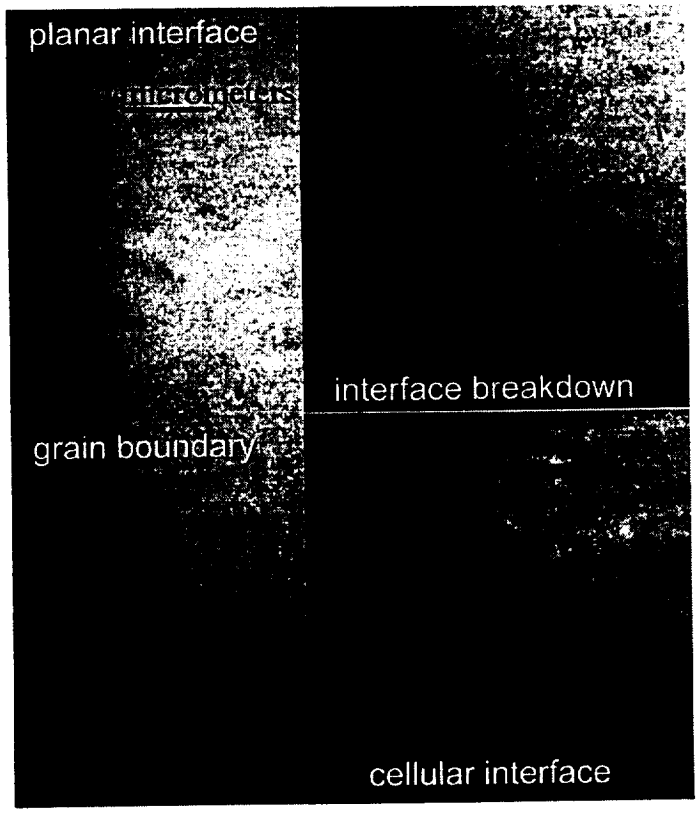

Figure 22. Al 2% Ag interfaces. Each are 2 second exposures at 55 kV acceleration and 200 μA current. Left figure shows planar interface growing at 1 μm/sec; grain boundaries intersect the interface isotherm. Upper right image captured the initial stages of cellular breakdown after the rate was increased to 2 μm/sec from 1.5 μm/sec. The lower right part shows the steady state cellular growth that followed at a continuous 2 μm/sec.

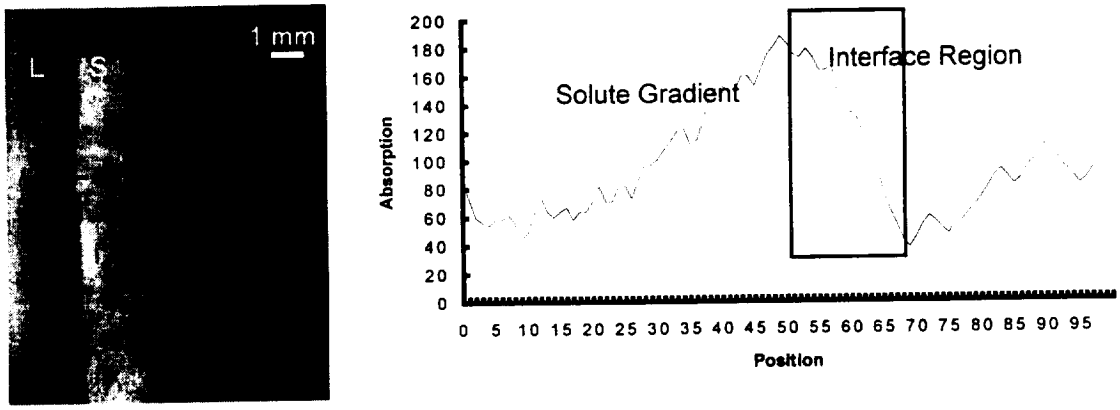

Figure 23. A) Al-18 In solid/liquid interface growing at 12.4 μm/sec in a 45 °C/cm temperature gradient showing solute rejection to the liquid after the step increase of translation rate. B) Optical intensity (absorption) profile along the line in A) crossing the solute layer and interface. Solute gradient is clearly seen on the left part of the graph. Increasing In content represents increased absorption. The diffuse interface region is in the marked area. Note the solute layer is not uniform along the length of the interface.

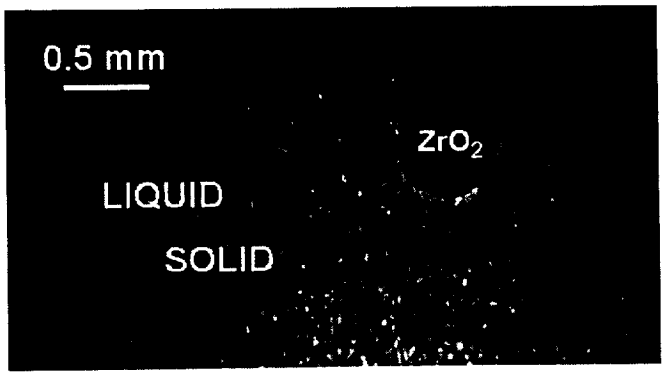

Growing (video) and stationary (radiograph) interfaces

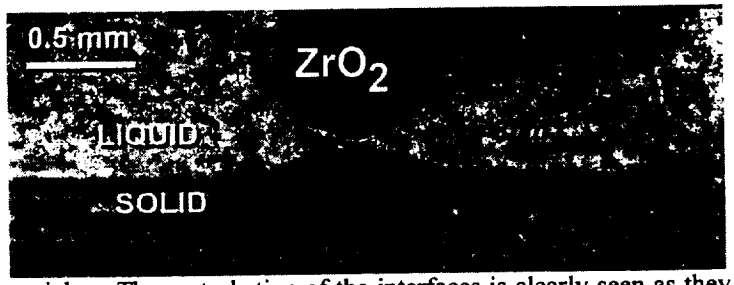

Fig 24 These are interfaces in Al near zirconia particles. The perturbation of the interfaces is clearly seen as they approach the particle. The lower conductivity of the particle causes the nearby solid to approach since it is shielded from the heat. The growing interface has less equivalent disturbance due to the release of heat of fusion all along the interface during the transformation from liquid to solid. The growing interface was captured with the intensifier and video, the stationary interface was captured on X-ray film.

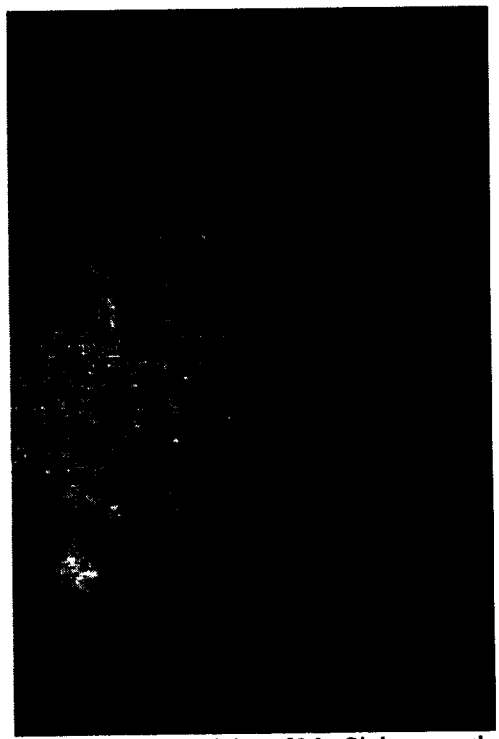

Figure 25. Al-Mn-Si in-situ during solidification. Particles of Mn-Si decorate the interface running up the middle of the picture. Solid is on the right and the growth direction is to the left. These precipitates were swept up by the interface and continue to grow as they are being pushed along. This is the first observation ever of particle pushing in a metallic system.

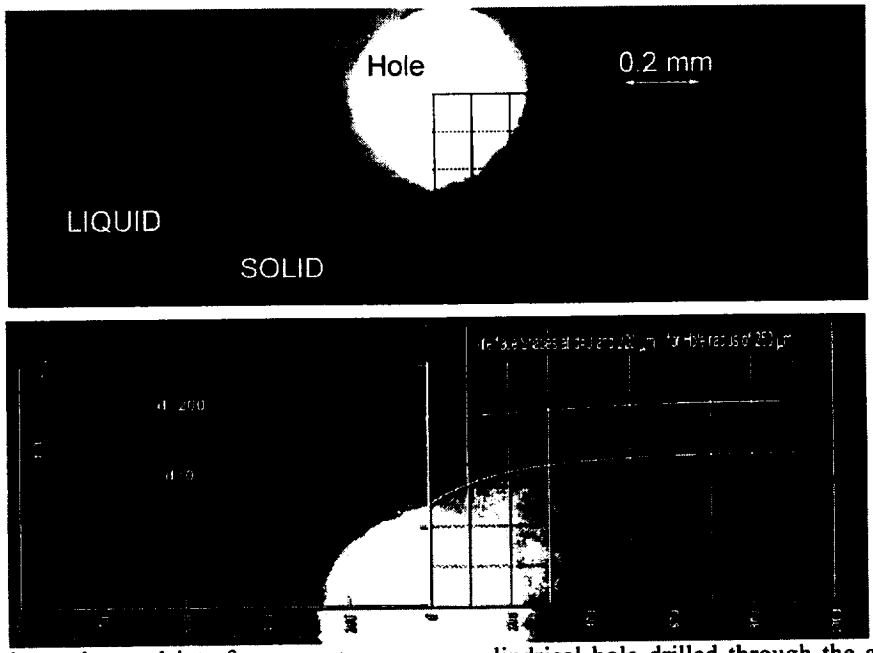

Fig. 26 Predicted vs. observed interface curvature near a cylindrical hole drilled through the aluminum. These stationary interfaces were radiographed on X-ray film and then digitized to permit superposition of the calculated interface shapes. The upper image shows good (but not perfect) matching while the lower image, where the interface is further from the hole, shows calculations of 200 and 250 μm gap. Neither calculated shape matches the interface very well. In general, the interface showed more curvature than the calculations. Reasonable adjustments of the thermal property data in the calculations could not bring the calculations into better agreement. Such comparisons have never been possible before.

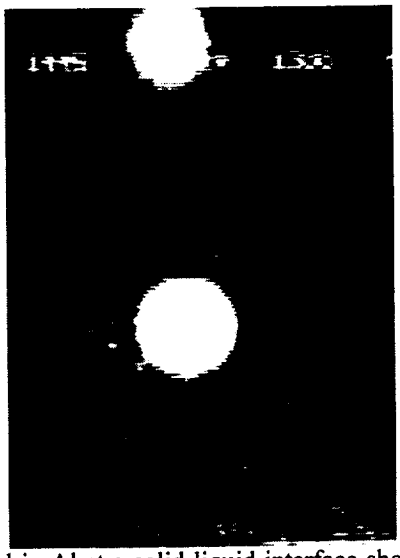

Fig. 27. A 250 μm and a 300 μm void in Al at a solid-liquid interface showing the local curvature caused by the low thermal conductivity of the voids. The interface is growing from right to left at 2 μm/sec in a 45 °C/cm temperature gradient. Interface interactions such as these occur frequently within castings as dissolved gasses collect into voids as they are rejected by the cooling liquid.

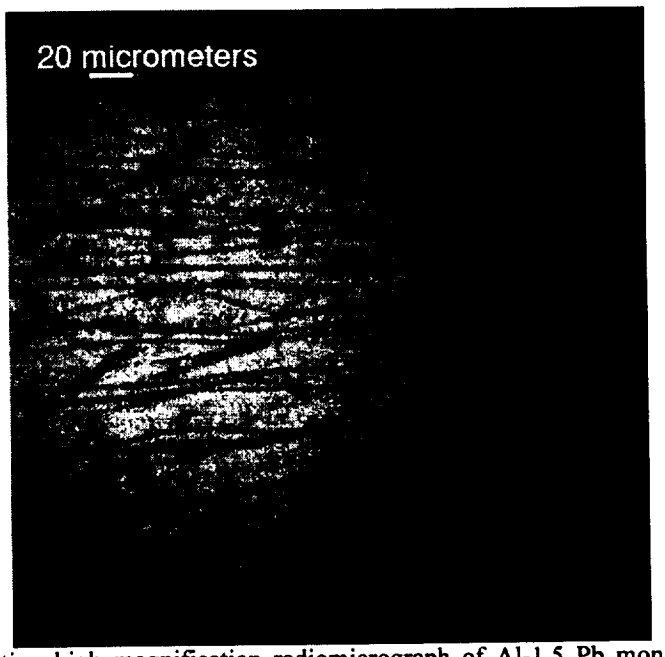

Figure 28. Post-solidification high magnification radiomicrograph of Al-1.5 Pb monotectic alloy showing fine fibers of Pb. This specimen was unidirectionally grown at 1 μm/sec in a temperature gradient of 45 °C/cm. The fibers can be seen to grow somewhat aligned on the left and meandering or twisting on the right due to some unknown phenomenon. Stereo imaging shows the twisting fibers spiraling in three dimensions amongst the other fibers.

Figure 29. Al-Pb monotectic radiograph showing periodic striations that developed within the sample. On the right is the darker section where the quench occurred during growth. These stria were regularly found in Al-In and Al-Pb monotectic specimens grown at appropriate rates. The darkening within the band is due to the increased local concentration of the solute within the volume of the specimen. The darkening occurs in this specimen with a periodic separation of 250 μm. Only by penetrating through the surface with X-rays can one detect these features since regular metallography cannot show these features. Once again, these observations were never made previously.

7.0 Distribution of Science and Technology Results to the Public and Scientific Community

7.1 Publications From This Project

Kaukler, W. F. and P. A. Curreri, "ADVANCEMENT OF X-RAY MICROSCOPY TECHNOLOGY AND IT'S APPLICATION TO METAL SOLIDIFICATION STUDIES," presented at the 1996 SPIE Technical Conference in Space Processing of Materials, Aug. 4, 1996; Proceedings Vol. 2809 p. 34.

William F. Kaukler and Peter A. Curreri, "REAL-TIME X-RAY TRANSMISSION MICROSCOPY OF SOLIDIFYING AL-PB ALLOYS," published in the "Eighth International Symposium on Experimental Methods for Microgravity Materials Science Research," The Metallurgical and Materials Society Annual Meeting, Anaheim, CA, Feb. 5, 1996

William F. Kaukler, Franz A. Rosenberger and Peter A. Curreri, "REAL-TIME X-RAY TRANSMISSION MICROSCOPY OF SOLIDIFYING AL-PB ALLOYS," Metallurgical Transactions (1997) in press.

Curreri, P.A., and W. Kaukler, "REAL-TIME X-RAY TRANSMISSION MICROSCOPY OF SOLIDIFYING AL-IN ALLOYS," Metallurgical and Materials Transactions A, 27A, pp. 801-808 1996.

Peter A. Curreri, and William F. Kaukler, "REAL-TIME X-RAY TRANSMISSION MICROSCOPY OF SOLIDIFYING AL-IN ALLOYS," published in Proceedings of the "Seventh International Symposium on Experimental Methods for Microgravity Materials Science Research," (presented at The Metallurgical and Materials Society Annual Meeting, Las Vegas, NV, Feb. 12-16, 1995) pp 93-101, The Minerals, Metals and Materials Society, 1995.

Curreri, P.A., and W. Kaukler, "X-RAY TRANSMISSION MICROSCOPY STUDY OF THE DYNAMICS OF SOLID/LIQUID INTERFACIAL BREAKDOWN DURING METAL ALLOY SOLIDIFICATION," Presented at 8th International Symposium on Experimental Methods for Microgravity Materials Science, Feb 4-8, 1996, Anaheim, CA, 125 TMS Annual Meeting.

Sen, S., W. Kaukler, P. Curreri, and D. M. Stefanescu, "DYNAMICS OF SOLID/LIQUID INTERFACE SHAPE EVOLUTION NEAR AN INSOLUBLE PARTICLE," Metallurgical Transactions 28A 1997.

S. Sen, D.M. Stefanescu, B.K. Dhindaw, W. Kaukler, P.A. Curreri: "THE RELEVANCE OF MICROGRAVITY TO THE INTERACTION OF A SOLIDIFYING PLANAR INTERFACE WITH AN INSOLUBLE PARTICLE."; in paper AIAA 97-0451, 35th Aerospace Sciences Meeting, Jan. 6-10, 1997, Reno, NV.

The abstract for a presentation was published in Microscopy Research and Technique vol. 28, page 452, 1994. The presentation was by Dr. Kaukler at the Thirteenth Annual Alabama Electron Microscopy Annual Meeting held at the Huntsville Hilton in Feb. 17 and 18, 1994.

7.2 Presentations

Dr. William F. Kaukler and Dr. Franz Rosenberger at the Alabama Materials Research Conference in Sept. 1993 at A & M University in Huntsville, AL.

Poster presentation by Dr. Kaukler at the Alabama Electron Microscopy Annual Meeting held at the Huntsville Hilton in Feb. 1994.

Another poster presented by Dr. P. A. Curreri, Dr. W. Kaukler and Dr. F. Rosenberger at the NASA Microgravity Materials Processing Conference held at the Von Braun Civic Center in Huntsville, AL in May 24-25, 1994.

W.F. Kaukler, F. Rosenberger, and P.A. Curreri, "Specimen Image Optimization of the X-ray Transmission Microscope", Eighth Annual Alabama Materials Research Conference, Tuscaloosa, Sept. 26 1994.

Gordon Conference on Gravitational Effects in Phisico-Chemical Systems.
Curreri and Kaukler. June 1995.

7.3 World Wide Web Pages

A series of 5 WWW pages have been prepared and placed on the net through the Marshall Space Flight Center Space Science Laboratory server in the Microgravity Materials Research area. The pages have been on-line for a year and have been updated and improved as the techniques for writing web pages improved. Hundreds of 'hits' per month to these pages are the norm and increase each month.

There are a few X-ray related home pages on the web throughout the world and some of the significant ones (National labs and Centers at universities) which do similar research have included our web site to link to.

These pages outline the project goals, explain the techniques, present meaningful results and demonstrate the benefits to the general public as well as materials scientists, metallurgists and microscopists.

A copy of the latest pages is included in the Appendix.

8.0 Design of an Orbital XTM facility

The Fein Focus Inc. (FF) High Definition X-ray system weighs about 3000 pounds and fills a small room. Clearly, this equipment cannot be flown in orbit. At the moment, there are no commercially available x-ray sources that offer the image quality of this FF system. X-ray tubes can be made that are much more compact and lighter in weight than this. Sealed microfocus x-ray tubes are commercially available and they offer 10 μm or less spot size. A sealed tube contains the electron gun, electrostatic focusing lenses and the tungsten target just like the FF system. The tube is small, made of ceramic or glass and has a permanent vacuum inside. The components are sealed within and the tube is disposed of once a part wears out. This is not unlike the vacuum tubes or picture tubes in TV sets. Sealed transmission tubes have been made in the past as research units and are being developed elsewhere. They consume little power due to their size (<50 watts). Since the tube characteristics are fixed over time, the high voltage supply can also be simplified and miniaturized. If a commercial microfocus x-ray tube (not transmission type) is used as a model for size and placement, one could add a compact furnace and a very compact x-ray camera system to assemble a small, lightweight XTM for space experiments. Figure 29 shows this concept schematically. Not including the control and imaging electronics on a small rack, this package as shown could easily weigh just 40-50 pounds and take less than 2 ½ X 1 X 1 feet of volume . The rack would contain x-ray source electronics and power, digital camera readout electronics, power for the furnace and a computer overseeing the whole system. Since the specimen can be small, the furnace can be small and have a low power consumption. With more time for designing the system for flight, and some lessons learned by testing a breadboard system, the weight and size can be reduced even further.

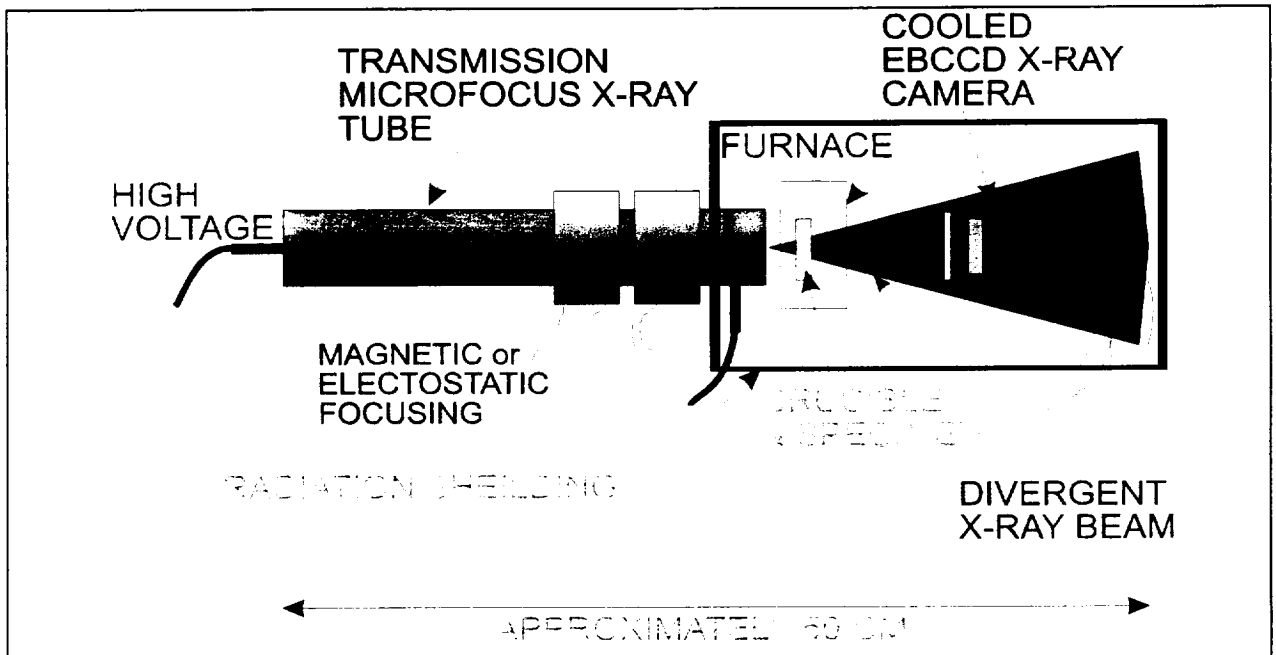

Figure 29. Schematic of orbital X-ray transmission Microscope for Solidification Studies

9.0 Comparison of Actual Progress with Project Schedule

During the first year (FY94) of this ATD tasks 1-6 of the original proposed project plan Milestone chart were completed as planned. Task 7 "Upgrade Converter" was addressed by experiments utilizing direct imaging with X-ray hardened CCDs. These test data were applied to the purchase of the advanced technology Converter/Intensifier for the third year (Task 13). Task 8, purchase of the advanced technology camera, was completed on time. Receipt of the camera was delayed due to delivery problems from the manufacturer. Task 9, purchase of the display system, was completed concurrent with Task 8. The advanced technology furnace construction, Task 10, was on track but required almost a year longer to make than expected. As outlined in this report, several generations of the furnace were constructed and the design philosophy had to be amended to achieve the goals. The high mag-high resolution furnace works very well but offers only a low thermal gradient with the aluminum alloys. In addition, long sample length was desired to reduce end effects, but is also conducive to prolonged 'burning' at the hot end of the sample. Task 11, Image solidifying metal, has been very satisfactorily achieved as is evident from figures found in this report.

Project Completion and Technology Success Criteria

*after 2 years will have breadboard system which can provide magnified X-ray images of solid-liquid interfaces in-situ in real time. **DONE**
*expect to have 100X images and achieve 3% density sensitivity although not necessarily at the same time on all specimens after 2 years. **DONE**
*during the first 2 years and most of the third, constant optimization of the working parameters of all components were to be established. **DONE**
*ability to make to make stereo X-ray images will be obtained in 2 years. Stationary specimens should provide stereo images after 3 years. **DONE** Stereo during solidification was the greatest challenge to meet. Real-time stereo was not affordable. Stereo images made in succession and viewed later were possible and worked well.

10. Summary and Conclusions

We have succeeded in meeting the goals set out in the proposal. A cadre of detector technologies is available to suit the requirements of the experiment. Resolutions of both real-time and absolute limits to resolution exceed the initial aspirations. Obtaining sufficient contrast is still a significant limitation but can be overcome by judicious selection of the specimen composition. This can only take time and trial and error for a successful result.

The 4^{th} generation furnace provides the capability of real-time in-situ observations of composite alloy development (as shown in the report). A low detection sensitivity however, has still made it difficult to observe dendritic growth, although it has been 'seen' in raw video; it was not a recordable signal.

We have examined flight ampoules with XTM to observe particle and thermocouple placement, crucible flaws and cracks in collaboration with the Particle Pushing and Engulfment flight experiment (Dr. Stefanescu, UA, P.I.). The value of an in flight XTM to guard against experiment failure and safety assurance is obvious.

Although not attributable to equipment limitations, a quest to observe particle pushing was not successful. We tried at length to prepare specimens that would demonstrate particle pushing. Instead, we were successful in imaging the interface deformation due to the thermal field distortion of a ceramic particle or void and to compare to calculated shapes. In theory, we should have been able to make major inroads to this field if the particles could be pushed and the velocities adjusted to make critical measurements. On the other hand, critical issues of sample preparation for the PEP flight experiment were established, particularly the clustering of particles and trapped voids. In this regard, the XTM did prove very useful so that flight specimens would work as expected and to perform post flight analysis. Although not a clear result, particle pushing of precipitates was observed in an Al-Si-Mn alloy. It may be that to be pushed, the particles need to be small and have clean surfaces like one might obtain from in-situ precipitation.

The ability to image features in real time will enable more fundamental and detailed understanding of solidification dynamics in microgravity than had previously been possible, thus, allowing the full benefits of microgravity experiments be applied towards rigorous testing of critical solidification models.

The XTM is also a valuable tool for post solidification metallography. The 3-dimensional distribution of solute and solidification features within the specimen volume can be viewed without sectioning or other treatment when the solute has sufficiently higher atomic mass than the solvent. Thus the XTM could provide the first practical method for on orbit microstructural (metallographic) analysis by the astronauts or by telescience.

END

Appendices

Prints from web pages.

X-ray Microscope for Metal Solidification Studies

NASA Microgravity Science and Applications Division &

The University of Alabama in Huntsville, CMMR

These pages (5 total) describe a new technique to directly observe the solidification (freezing) process in metal alloys in real-time by using x-rays. In the following pages you will find: images and explainations of what we can see, how it's done, and what we plan. Our method of X-ray Microscopy uses a special microfocus x-ray source to create images of the solid-liquid interface *during* solidification under controlled conditions. Features having dimensions below ten micrometers are being observed and studied in real-time. The information from this fundamental research is used to produce stronger alloys and composite materials. In addition, every experiment is an exploration into previously unseen worlds.

The first example, above, shows the kind of interesting internal structures we can observe. This is a low magnification post-solidification x-ray micrograph of an aluminum-indium monotectic alloy unidirectionally solidified (from right to left) while the level of gravity was cycled up and down (along the long axis of the specimen) from 1.8 to 0.01 times earth gravity. This was done by flying the furnace in a NASA aircraft flown in a special, parabolic trajectory to simulate the low gravity conditions in space for 20 seconds at a time. Much more can be found about these aircraft at NASA Lewis Research Center.

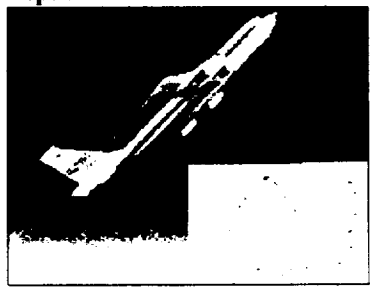

The distribution of the indium particles that formed during the solidification are periodically clustered in response to the level of gravity imposed. (The specimen is 5 mm in diameter.) Such solidification studies are an example of the kind of research that NASA's Microgravity Science and Applications Division is responsible for. The X-ray Microscope is presently too large to use in a microgravity environment but the XTM is used to examine flight samples before and after the experiments are run on the Shuttle. We are presently designing a compact version that could be tested on the KC-135. Examples of x-ray microscopy *during solidification* of aluminum alloys (in the laboratory) using the X-ray Transmission Microscope (XTM) can be found on the next page.

This work is being performed by Dr. William Kaukler and Dr. Peter Curreri at Marshall Space Flight Center in Huntsville, Alabama.

What We Can Do

We (Dr. Peter A. Curreri of National Aeronautics and Space Administration at Marshall Space Flight Center and D F. Kaukler of the Center for Microgravity and Materials Research at The University of Alabama in Huntsville) are u high resolution x-ray microscope to view, in-situ and in real time, interfacial processes in metallic systems during fr Studies of this type are not being performed anywhere else. The instrument is in the background of the picture.

~~~~ Picture gallery of microradiographs are below ~~~~

For bigger images, click on the pictures.

In the field of materials science it is well known that many of the properties of a material stem from the structure of that material. During the last century, by examining metal alloys with an optical microscope after polishing and etching the surface, it was discovered that the microstructures influenced the material's properties. The initial microstructure forms during the casting process where the melted alloy becomes a crystalline solid. In various ways, 80% of ALL industry involves a casting or solidification process of a material. Clearly it is important to understand this subject.

Physical processes which occur at, or near, the solid-liquid interface during solidification lead to a variety of patterned structures or morphologies. These interfacial morphologies account for the various microstructures found in alloys partly due to the composition and partly to the solidification conditions. Certain tricks were required to see these interfacial structures while they formed since people could not see inside a metal as it solidified. One trick was to quench the material and rapidly freeze the interface shape to be later seen upon sectioning (metallography). Another trick was to decant (pour off) the molten metal that had not yet solidified and leave behind the solid part of the interface structure. The best trick was to not use metal at all, but instead study the solidification of transparent organic *models* for metallic solidification. Every trick used still couldn't show exactly what's going on during this transformation of liquid to crystalline solid. In addition, little information was obtained about the dynamics of the processes.

The X-ray Transmission Microscope (XTM), in the Space Sciences Laboratory, MSFC, operates in the hard x-ray range (10 to 100 keV) and achieves magnification through projection. (explained later). We have obtained, using aluminum alloys, real-time images of the evolution of interface morphologies with characteristic lengths as small as 50 μm (50 micrometers), interfacial solute accumulation and formation of droplets (5 μm). We are addressing the complex issues of resolution, contrast and minimal exposure time and improving the capability of the XTM.

Some radiographs of alloys captured during solidification are presented below.

The next web page shows how it is done.

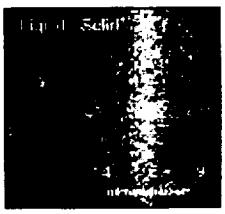

Interface of Aluminum-Lead (Al-Pb) alloy showing liquid (dark left side) and solid. Solidification is progressing from right to left. The solid portion on the right shows three regions with different growth rates as marked. The band structure in the solid (zebra stripes vertical) changes spacing with this growth rate change. The liquid near the solid is quite dark due to the accumulation of the dense lead (Pb) in the liquid. This is a solute layer formed by the rejection of the lead by the solid and can only diffuse away into the liquid away from the interface. This rejection is a normal solidification phenomenon but has never been photographed before in a metal alloy.

For bigger images, click on the pictures.

Interface of Aluminum-2% Silver (Al-Ag) alloy showing liquid (melt) on the left side and solid Al 'fingers' on the right. Solidification is progressing from right to left. This interface has what is called a cellular morphology. Constitutional undercooling (solidification phenomenon in alloys) brought on by the solute (Ag) buildup during solidification lead to the formation of these fingers of Al surrounded by Ag-rich melt. These cells are about 75 μm across. Since the cells are so small, they overlap in layers and it is not easy to delineate them except when you are lucky find a clean area like here. The growth rate is 2 μm/sec. The image was taken with a 2 second exposure with 55 kV acceleration and 200 μA input current.

For bigger images, click on the pictures.

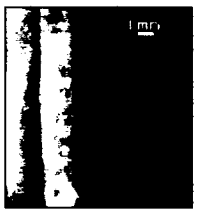

Interface of Aluminum-Indium (Al-In) alloy showing how the Indium solute is collecting ahead of the solid in the liquid region during growth as solidification progresses from right to left. The dark cloud to the left of the interface is this solute layer in the liquid (melt). The darker portion on the right was solidified at a slower rate than the light colored part between the interface and this darker region. It is this higher growth rate that is causing the more solute to be collected ahead of the interface in the liquid instead of being deposited in the solid thus making the solid 'lighter' or less absorbing to x-rays.

For bigger images, click on the pictures.

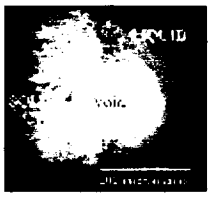

Interface of Aluminum-2% Silver (Al-Ag) alloy about to engulf a gas bubble that formed in the melt. The interface itself is growing with a cellular structure due to the build-up of silver in the melt resulting in constitutional supercooling that leads to the interface breakdown. (See also image above.) The extra silver in the liquid accounts for the darker appearance of the melt and in the cell walls. This is the first image of its kind showing the growing cellular interface AND the engulfment of the void. The growth rate is 2 μm/sec and the thermal gradient is 47 degrees C per centimeter.

X-ray Microscope for Metal Solidification Studies

How to Do Hard X-Ray Microscopy:

With metallic and semiconducting samples, the penetration of macroscopic layers requires photon energies in excess of 10 keV. This precludes the use of optical approaches for imaging. Only projection radiography can be employed in this energy range to see through hot and molten metals. Projection radiography uses the divergence of the beam from a small source. The ultimate resolution is limited by the diameter of the source. Hence, x-ray projection radiography requires micro-focus x-ray tubes. Our X-ray Transmission Microscope (XTM) utilizes one of the smallest micro-focus sources commercially available. The spot size (electron beam focus on the target) is set down to around a one micrometer diameter.

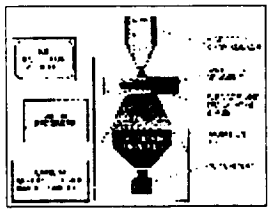

For bigger images, click on the diagrams.

This figure schematically indicates the major components of the system and their placement. A metal sample (one mm thickness) is contained in a specially designed, high transmittance crucible. A furnace on a translation stage imposes a temperature gradient onto the sample (one end molten, the other solid). The solid-liquid interface is positioned in close proximity to the focal spot of a micro-focus x-ray source. The diverging x-ray beam permeates the sample and the resulting shadow falls on an x-ray image intensifier. The resulting visible image is converted to a digital image by a CCD camera and stored in a computer. This image is displayed on a high resolution monitor, either in real time or after further processing (contrast enhancement, filtering, etc.).

For bigger images, click on the diagrams.

This diagram shows how the x-ray shadow of an object is magnified by projection. The rays emanate from the irradiated spot such that each portion of the spot casts its own shadow. The merged shadows from all areas of the spot form the final projected image. The diagram shows the broadening of features from the specimen plane onto the projection plane. The finite source spot size limits the resolution of the image. Magnification is established by the ratio of a + b to a. This method of microscopy produces infinite depth of field since no focusing is required.

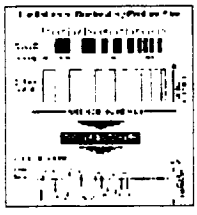

The limit to image contrast (equally important to resolution) is examined in this figure. Here, the x-ray shadow (image) is formed from a specimen of different sized features which (for simplicity) are fully absorbing (or black). The shadow on the detector is converted to a visible light image which shows the features with differing amounts of darkness depending on their size. The problem is that very small small features can disappear because their signal is too low (below noise level). This is the contrast transfer function which limits the ability to image small features. This limitation is established by the image conversion and detection processes. Technology improvements to the XTM are best concentrated in this area.

At typical solidification rates, motion-induced blurring limits the exposure time to less than a few seconds. With state-of-the-art x-ray image intensifier/camera combinations, which have a spatial resolution of order 100 μm (100 micrometers), a magnification on the intensifier input window of some 20X is required to obtain a spatial resolution of 10 μm. Such resolution is needed to see the dendritic structures formed in some solidifying metals. (See Related Web Sites for info regarding dendrite structures.) Since magnification is the direct ratio of detector-source to specimen-source distances, magnifications of 20X or more will require the (heated) specimen to be less than 1 cm from the housing of the x-ray tube. This leaves little room for the crucible, insulation and cooled housing creating challenging design problems for the x-ray furnace.

Of course, such observations require sufficient contrast (difference in absorptance) between features to be resolved and the retention of this contrast by the imaging devices (image intensifier, camera, recording device). In monocomponent metallic systems, contrast between solid and melt is determined by the (electron cloud) density of the two phases resulting in less than 2% radiographic (image) contrast. [This low contrast is the main limit to the more universal application of this form of study.] In alloy systems, solute segregation will lead to further contrast enhancement. The magnitude of contrast is proportional to the difference in atomic number of the components and

their concentration.

How much of the original image contrast is retained, depends on the dynamic range of the detector (imaging train) and the size of the features in the object. For small length scales, the contrast retained by the imaging train becomes much smaller than the original image contrast. (This phenomenon was described above.) This can only be (partly) compensated for if the dynamic range of the imaging train is high enough and that the lowest intensities of interest remain above the noise of the system.

What Can We Do? | **What We Plan to Do** | **Related Web Sites** | **Back to X-ray Homepage** | **Contacts**

Last Updated Dec. 5, 1996